The surface aerosol optical properties in urban areas of Nanjing, west Yangtze River Delta of China

B. L. Zhuang[1, *], T. J. Wang[1, **], J. Liu[1, 2], S. Li[1], M. Xie[1], Y. Han[1], P. L. Chen[1], Q. D. Hu[1], X.-Q. Yang[1], C. B. Fu[1], J. L. Zhu[3]

[1] School of Atmospheric Sciences, CMA-NJU Joint Laboratory for Climate Prediction Studies, Jiangsu Collaborative Innovation Center for Climate Change, Nanjing University, Nanjing 210023, China

[2] Department of Geography and Planning, University of Toronto, Toronto, M5S 3G3, Canada

[3] Department of Climate and Space Sciences and Engineering, University of Michigan, Ann Arbor, Michigan, USA

[*] Corresponding author, E-mail: blzhuang@nju.edu.cn; Tel.: +862589681156; fax: +862589683797

[* *]Corresponding author, E-mail: tjwang@nju.edu.cn; Tel.: +862589683797; fax: +862589683797

Abstract: Observational studies of aerosol optical properties are useful to reducing uncertainties in estimating aerosol radiative forcing and forecasting visibility. In this study, the observed near-surface aerosol optical properties in urban Nanjing are analyzed from Mar 2014 to Feb 2016. Results show that near-surface urban aerosols in Nanjing are mainly from local emissions and the surrounding regions. They have lower loadings but are more scattering than aerosols in most cities in China. The annual mean aerosol extinction coefficient (EC), single scattering albedo (SSA) and asymmetry parameter (ASP) at 550 nm are 381.96 Mm^{-1}, 0.9 and 0.57, respectively. The aerosol absorption coefficient (AAC) is about one order of magnitude smaller than its scattering coefficient (SC). However, the absorbing aerosol has larger Ångström exponent (AAE) value, 1.58 at 470/660 nm, about 0.2 larger than the scattering aerosols' (SAE). All the aerosol optical properties followed a near unimodal pattern, the ranges around their averages accounting for more than 60% of the total samplings. Additionally, they have substantial seasonality and diurnal variations. High levels of SC and AAC all appear in winter due to higher aerosol and trace gas emissions. AAE (ASP) is the smallest (largest) in summer because of

high relative humidity (RH) which also causes considerably larger SC and smaller SAE, although intensive gas-to-particle transformation could produce a large number of finer scattering aerosols in this season. Seasonality of EC is different from the columnar aerosol optical depth. Larger AACs appear at the rush hours of the day while SC and back scattering coefficient (Bsp) only peak in the early morning. Aerosols are fresher at daytime than at nighttime, leading to their larger Ångström exponent and smaller ASP. Different temporal variations between AAC and SC cause the aerosols more absorbing (smaller SSA) in autumn and around rush hours. ASP has a good quasi-LogNormal growth trend with increasing SC when RH is below 60%. The correlation between AAC and SC at the site is close but a little smaller than that in suburban Nanjing in spring. Atmospheric visibility decreases exponentially with increasing EC or SC, more sharply in spring and summer, and it could be further deteriorated with increasing SSA and ASP.

1 Introduction

Atmospheric aerosols have substantial influences on human health, air quality and climate changes and their loadings have significantly increased since the preindustrial times (Qin et al., 2001; Forster et al., 2007). Due to their ability of scattering/absorbing solar radiation and acting as cloud condensation nuclei, atmospheric aerosols can affect atmospheric radiation and dynamics, as well as the Earth's hydrologic cycle, leading to regional or global climate changes (Forster et al., 2007; Rosenfeld et al., 2008; Qian et al., 2009; Li et al., 2011; Wang et al., 2014; Guo et al., 2016a). Light scattering aerosols have contributed to offsetting the warming effect of CO_2 (Kiehl and Briegleb 1993) while light absorbing aerosols such as black carbon (BC) could further enhance the global warming (Jacobson 2002), especially in the high aerosol regions. Due to the warming effect of BC, the atmosphere would

47 become more unstable, which might result in the changes in the trend of precipitation in China over the
48 past decades as suggested by Menon et al. (2002). Furthermore, atmospheric aerosols can be a major
49 component in haze pollution, altering atmospheric visibility and being harmful to human health
50 (Chameides and Bergin, 2002).

51 Observations and modeling studies have been conducted on aerosol optical properties and
52 radiative forcing, as well as its climate effects on regional and global scales in the past two decades
53 (e.g., Penner et al., 2001; Bellouin et al., 2003; Liao and Seinfeld, 2005; Yan et al., 2008; Wu et al.,
54 2012; Zhuang et al., 2013a; 2014a; Wang et al., 2015; Yu et al., 2016). Forster et al. (2007) summarized
55 that large uncertainties exist in estimating the aerosol radiative forcing, especially in climate models.
56 The bias mostly results from the uncertainties in the simulated aerosol optical properties (Holler et al.,
57 2003), which, in turn, are related to the aerosol loadings, profiles, compositions, mixing states and the
58 atmospheric humidity. The 5th IPCC reported that the global mean direct radiative forcing ranged from
59 -0.85 to +0.15 W m^{-2} for total aerosols and from +0.05 to +0.8 W m^{-2} for BC (IPCC, 2013). This would
60 further lead to much larger uncertainties in the estimations of the aerosol climate effects. In East Asia,
61 the range of simulated BC direct radiative forcing is much larger than the global one, varying from
62 +0.32 to +0.81 W m^2 (Zhuang et al., 2013a). The uncertainty could be substantially reduced in a model
63 if the aerosol optical properties are based on the observations or if the observed properties are directly
64 used (Forster et al., 2007).

65 In the last three decades, China has experienced the rapidest economic growth among countries in
66 East Asia and even the world. This leads to high emission of aerosols and trace gases (e.g., Guo et al.,
67 2009; Zhang et al., 2009; Xin et al., 2014; Che et al., 2015). The anthropogenic aerosol emissions in
68 East Asia were estimated to exceed 1/4 of the global emissions (Streets et al., 2001), resulting in more

diversified aerosol compositions, complex species and heterogeneous spatial distributions in the region (Zhang et al., 2012), especially in megacities and urban agglomerations (e.g., Beijing-Tianjin-Hebei (BTH), Yangtze River Delta (YRD) and Pearl River Delta (PRD) regions). Uncertainties of the aerosol radiative forcing and corresponding climate effects in these regions might be much larger than those of the rest of the world (e.g.: Forster et al., 2007 and Zhuang et al.,2013b). In addition, the diurnal variability of aerosol properties has been suggested to another major factors leading to such large biases (e.g., Xu et al., 2016). Therefore, it is necessary to characterize the aerosol optical properties based on observations in China, as did many studies in recent years at urban sites and in rural areas (e.g., Bergin et al., 2001; Xu et al., 2002; 2004; Zhang et al., 2004; Yan, 2006; Xia et al., 2007; Li et al., 2007; Yan et al., 2008; Andreae et al., 2008; He et al., 2009; Wu et al., 2009; Wang et al., 2009; Li et al., 2010; Fan et al., 2010; Bai et al., 2011; Cai et al., 2011; Xiao et al., 2011; Xu et al., 2012; Wu et al., 2012; Zhuang et al., 2015; Zhang et al., 2015; Li et al., 2015a; b; Yu et al., 2016). For example, Bergin et al. (2001), He et al. (2009) and Zhuang et al. (2015) presented the surface aerosol scattering and absorption properties in urban area of North and East China and they suggested that the annual mean 532 nm-AAC in Beijing was about 56 Mm^{-1} and it was 41~44 Mm^{-1} in YRD, which were much smaller than those in central to southwest China and in PRD (Wu et al., 2009; Cao et al., 2012; Tao et al., 2014) but much larger than those in rural and desert region (Xu et al., 2002; 2004; Yan et al., 2008). In addition to surface measurements, the columnar optical properties of the aerosols were also observed (Xia et al., 2007; Zhuang et al., 2014a; Che et al., 2015). Long-term measurements of the countrywide-aerosol optical depths and Ångström exponents in China from 2002 to 2013 were introduced by Che et al. (2015). In spite of substantial observation-based studies mentioned, measurements and analysis on aerosol properties in YRD region, one of the most populous regions in

China, is still rather limited. To fill the gaps in the current observational network in China and to better understand the optical properties of urban aerosols in YRD, this study will analyze the observations of aerosol scattering (SC), back scattering (Bsp), absorption (AAC), extinction (EC) coefficients and single scattering albedo (SSA), Ångström exponent of scattering (SAE) and absorbing (AAE) aerosols, as well as aerosol asymmetry parameter (ASP) in urban area of Nanjing, a major megacity in YRD. Our ultimate goals are to provide a reference when estimating aerosol radiative forcing and climate effect as well as forecasting visibility.

In the following, the method is described in Section 2. Results and discussions are presented in Section 3, followed by Conclusions in Section 4.

2 Data and Methodologies

2.1 Sampling station and instruments

The sampling station is located at the Gulou campus of Nanjing University, urban area of Nanjing (32.05^{o} N, 118.78^{o} E). It is built on the roof of a 79.3 m-tall building, around which there are no industrial pollution sources within a 30-km radius but there are several main roads with apparent traffic pollution, especially at rush hours. The layout of the site and the corresponding climatology have been described in Zhu et al. (2012).

The wavelength dependent aerosol absorption coefficient (AAC) and concentrations of black carbon (BC) were derived from the measurements using a seven-channel Aethalomter (model AE-31, Magee Scientific, USA). The wavelength dependent aerosol scattering coefficient (SC) and back scattering coefficient (Bsp) were measured by a three-wavelength integrating Nephelometer (Aurora 3000, Australia). To make a brief comparison between surface and column aerosols, the wavelength

dependent columnar aerosol optical depth (AOD) was observed using a Cimel sunphotometer (CE-318). The AE-31 model measures light attenuation at seven wavelengths, including 370, 470, 520, 590, 660, 880, and 950 nm, respectively, with a desired flow rate of 5.0 L/min and a sampling interval of 5 min. Aurora 3000 measures the aerosol's light scattering, including SC and Bsp at 450, 525 and 635 nm, with a sampling interval of 1 min. CE-318 measures the AOD from 340 to 1640 nm at day times. Routine calibrations and maintenances were carried out for all these instruments during the sampling periods. R-134 was used as a span gas for Aurora 3000. The aerosol inlet is located about 1 m above the roof. Data to be analyzed in this study were measured from Mar 2014 to Feb 2016 for AE-31 and CE-318 and from Jun 2014 to Feb 2016 for Aurora 3000. Meteorological data (such as relative humidity) during the sampling period are from the National Meteorological Station of Nanjing (No. 58238).

2.2 Calculation of the aerosol optical properties

The wavelength dependent aerosol absorption coefficient (AAC) and BC mass concentration can be calculated directly based on the measured light attenuations (ATN) through a quartz filter matrix (Petzold et al., 1997; Weingartner et al., 2003; Arnott et al., 2005; Schmid et al., 2006):

$$\sigma_{\mathrm{ATN},t}(\lambda) = \frac{(\mathrm{ATN}_t(\lambda) - \mathrm{ATN}_{t-1}(\lambda))}{\Delta t} \times \frac{A}{V} \quad (1)$$

where A (in m^2) is the area of the aerosol-laden filter spot, V is the volumetric sampling flow rate (in L/min) and Δt is the time interval (=5 min) between *t* and *t-1*. σ_{ATN} is the AAC without any correction, which is generally larger than the actual one (σ_{abs}) because of the optical interactions of the filter substrate with the deposited aerosol. Generally, there are two key factors leading to the bias: 1) multiple scattering of light at the filter fibers (multiple scattering effect), and 2) instrumental response

with increased particle loading on the filter (shadowing effect). Thus, the correction is needed and the calibration factors *C* and *R* (shown in Eq. 2) are introduced to against the scattering effect and shadowing effect, respectively:

$$\sigma_{\mathrm{abs},t}(\lambda)=\frac{\sigma_{\mathrm{ATN},t}(\lambda)}{C\times R} \tag{2}$$

Collaud Coen et al. (2010) suggested that AAC corrected from Weingartner et al. (2003) (WC2003 for short, hereinafter) and Schmid et al. (2006) (SC2006 for short, hereinafter) have good agreements with the one measured by a Multi-Angle Absorption Photometer. These two corrections are similar to each other and they use the same $R(\lambda)$:

$$R_t(\lambda)=(\frac{1}{f}-1)\times\frac{\ln(\mathrm{ATN}_t(\lambda))-\ln 10}{\ln 50-\ln 10}+1 \tag{3}$$

where R =1 when $\mathrm{ATN}\le 10$ and f =1.2. However, C value is fixed in WC2003 while is wavelength dependent in SC2006. According to Wu et al. (2013) and Zhuang et al. (2015), C in Nanjing is 3.48 in WC2003 while it is 2.95, 3.37, 3.56, 3.79, 3.99, 4.51 and 4.64 at 370, 470, 520, 590, 660, 880, and 950 nm, respectively, in SC2006. Zhuang et al. (2015) further suggested that wavelength dependent AACs corrected by SC2006 might be more close to the real ones than WC2003's in Nanjing, although 532 nm-AACs from these two corrections are close to each other. In addition to the direct way, AAC can also be calculated indirectly:

$$\sigma_{\mathrm{abs},t}(\lambda)=[BC]\times\gamma \tag{4}$$

where [BC] is the mass concentration of Aethalometer BC (in μg/m^3) without any correction and γ is the conversion factor determined empirically from linear regression of the Aethalometer BC concentration versus the aerosol absorption measurement (Yan et al., 2008). Zhuang et al. (2015) indicated that γ from the linear regression of the Aethalometer BC concentrations (ng/m^3) at 880 nm

against the light absorption coefficient (Mm^{-1}) at 532 nm in Nanjing is about 11.05 m^2/g. It's obviously that only 532 nm-AAC can be addressed from this way. Thus, AACs corrected from SC2006 are used in this study.

Based on wavelength dependent AAC and SC, Ångström exponent of scattering (SAE) and absorbing (AAE) aerosols are estimated as followed:

$$AAE_{470/660\text{nm}} = -\log(AAC_{470nm} / AAC_{660nm}) / \log(470/660) \quad (5)$$

$$SAE_{450/635\text{nm}} = -\log(SC_{450nm} / SC_{635nm}) / \log(450/635) \quad (6)$$

For purposes of comparison, AAC at 450, 525, 532, 550 and 635 nm, SC at 532 and 550 nm as well as Bsp at 532 and 550 nm were further calculated by the given coefficients and corresponding Ångström exponents:

$$\sigma_\lambda = \sigma_{\lambda_0} \times (\frac{\lambda}{\lambda_0})^{-\alpha} \quad (7)$$

where, σ_λ is the coefficient at wave length λ, α is the corresponding Ångström exponents.

Based on wavelength dependent SC, Bsp, AAC, aerosol asymmetry parameter (ASP), single scattering albedo (SSA) and extinction coefficient (EC) are further estimated:

$$ASP_\lambda = -7.143889\beta_\lambda^3 + 7.46443\beta_\lambda^2 - 3.9356\beta_\lambda + 0.9893 \quad (8)$$

$$SSA_\lambda = \frac{SC_\lambda}{SC_\lambda + AAC_\lambda} \quad (9)$$

$$EC_\lambda = SC_\lambda + AAC_\lambda \quad (10)$$

where, β_λ is the ratio of Bsp to SC at wavelength λ. Eq. 8 derives from Andrews et al. (2006).

3 Results and discussions

It's well known that the temporal variations of the aerosol optical properties at different

177 wavelengths are generally consistent with each other. Therefore, only single wavelength (such as 550
178 nm) AAC, SC, Bsp, SSA and ASP are focused when analyzing their basic characteristics (including
179 temporal variations, frequency distributions and changes with wind direction), their relationships with
180 each other, and their relationships with the meteorological conditions (such as RH and VIS) and
181 columnar AOD.

182 **3.1 Temporal variations of the aerosol optical properties**

183 The aerosol absorption coefficient (AAC) was directly obtained from the measurement of AE-31
184 and the scattering and back scattering coefficients (SC and Bsp), which were directly measured from
185 Aurora 3000. Based on wavelength dependent AAC and SC, Ångström exponent of absorbing (AAE at
186 470/660 nm) and scattering (SAE at 450/635 nm) aerosols were estimated according Eq.5 and Eq. 6,
187 respectively. Based on AAC, SC and Bsp, wavelength dependent aerosol asymmetry parameter (ASP),
188 single scattering albedo (SSA) and extinction coefficient (EC) are further estimated using Eqs. 8~10
189 and analyzed. Table 1 lists the statistical summary of surface aerosol optical properties in urban area of
190 Nanjing during the sampling period. The annual mean AAC, SC, Bsp, EC, SSA and ASP at 550 nm,
191 AAE at 470/660 nm and SAE at 450/635 nm is 29.615 Mm^{-1}, 338.275 Mm^{-1}, 44.257 Mm^{-1}, 381.958
192 Mm^{-1}, 0.901, 0.571, 1.583 and 1.320, respectively, with a standard deviation of 20.454 Mm^{-1}, 228.078
193 Mm^{-1}, 27.396 Mm^{-1}, 252.271 Mm^{-1}, 0.049, 0.088, 0.228 and 0.407, respectively.

194 **Table 1**

195 Figure 1 shows the 10th, 25th, median, 75th and 90th percentile values of the 550 nm- AAC, SC,
196 Bsp, 470/660 nm-AAE and 450/635 nm-SAE in urban area of Nanjing in each season from Mar 2014
197 to Feb 2016. Default values of aerosol scattering properties in spring 2014 are blank because the
198 measurements of Aurora 3000 started from June 2014. The figure suggests that AAC, SC, Bsp, AAE

and SAE have substantially seasonal variations. High level of AAC appears in winter times (DJF) while the lower one is found in summer (JJA) (Fig. 1a). The temporal trend of Bsp is similar to AAC's (Fig. 1d). According to Zhang et al. (2009), emissions of the aerosols and trace gases in China are larger in winter than in the other seasons especially for carbonaceous aerosols (Fig. 1c in Zhuang et al., 2013b). Thus, the higher AAC values in winter than in summer might result from the higher aerosol emissions, lower boundary height (Guo et al., 2016b) and less rainfall. However, possibly due to the impacts of hygroscopic growth of aerosol caused by higher RH in summer and dust aerosol in spring (Zhuang et al., 2014a), SC is considerably large in these two seasons (Fig. 1c). Thus, the lowest SC is found in autumn in both 2014 and 2015. AAE has seasonality similar to AAC. Due to relatively higher RH, small value of AAE is found in JJA while the larger ones appear in the other seasons (Fig. 1b), which is different from the seasonality of SAE. SAE is larger in warmer seasons but is smaller in the other seasons. Scattering aerosols, including inorganic and partially organic components, mainly come from gas-to-particle transformation, so that they have smaller sizes (larger AE) compared to the primary aerosols (such as dust and BC). The efficiency of gas-to-particle transformation is higher in warmer seasons. The observations of the aerosol compositions at the site showed that seasonal mean inorganic aerosols, including sulfate, nitrate and ammonium, account for about 50% of the total $PM_{2.5}$ in spring and might be higher than 50% in the other seasons (Zhuang et al., 2014b). Thus, SAE in summer and autumn is large (Fig. 1e). RH can impose substantial influences on scattering aerosols. SAE might be much larger than the current values in these two seasons if the hygroscopic growth were excluded. Seasonal mean RH is about 75.41% and 70.86% in JJA and SON, respectively, to a certain degree leading to higher values of SAE in autumn than in summer. The figure also suggests that aerosol absorption coefficient and scattering coefficient as well as their sizes in 2014 are higher than those in

2015. The observed RH difference in these two years at least partly accounts for the variation of aerosol absorption coefficient and scattering coefficient as well as their sizes. A comparison of RH between 2014 and 2015 indicates that RH is 79.49% and 72.86% in JJA and SON, respectively, in 2014, larger than that in 2015 (71.33% in JJA and 69.03 in SON).

Figure 1

Figure 2 plots the seasonal mean values with standard deviations of AAC, SC, Bsp, EC, SSA, ASP, AAE at 470/660 nm and SAE at 450/635 nm. AAC, SC, Bsp and EC increase with decreasing wavelength in four seasons. Changes in SSA and ASP with increasing wavelength are different in different seasons. SSA increases with increasing wavelength in colder seasons but little in JJA and SON. ASP increases with wavelength in JJA, opposite to in other seasons. The figure also suggests that seasonal variation of EC is more consistent with SC's, with large values in JJA and DJF (370.236 and 422.569 Mm^{-1}, respectively, at 550 nm). The largest values of SSA and ASP appear in JJA (0.933 and 0.638, respectively, at 550 nm), implying that aerosols in urban area of Nanjing are more scattering and have stronger forward scattering ability in JJA than in other seasons. The urban aerosols are more absorbent in SON in Nanjing (550 nm SSA is about 0.874).

Figure 2

Seasonal mean 550 nm AAC, SC, Bsp, EC, SSA, and ASP, 470/660 nm AAE and 450/635 nm SAE as well as corresponding standard deviations are listed in Table 2. It suggests that seasonal mean 550 nm AAC, SC, Bsp, EC, SSA, and ASP vary from 19.65 to 37.96 Mm^{-1}, 294.62 to 385.14 Mm^{-1}, 36.99 to 54.79 Mm^{-1}, 341.3 to 422.57 Mm^{-1}, 0.874 to 0.933, and 0.54 to 0.64, respectively. Seasonal mean AAE and SAE vary from 1.49 to 1.70 and 1.1 to 1.54, respectively. AAC and Bsp in DJF are about 2 and 1.5 times of those in JJA, respectively. SSA in JJA is about 6.75% larger than that in SON.

Table 2

In addition to seasonality, the aerosol optical properties near the surface at urban Nanjing have substantial diurnal variations (Figure 3), especially for the coefficients (AAC, SC, Bsp and EC). The diurnal variation of EC, which is consistent with SC, is not showed in the figure. AAC levels are usually high at the rush hours around 07:00-09:00 am and around 09:00-11:00 pm but low in the afternoon (Fig. 3a). At 08:00 am, mean 550 nm-AAC is as large as about 34 Mm^{-1}, while at 02:00 pm, it is about 23 Mm^{-1}. SC and Bsp (Fig. 3b and 3c), to some extent, have diurnal variations similar to AAC's. Their lowest values also appear in the afternoon (about 280 Mm^{-1} for SC and 38 Mm^{-1} for Bsp). However, only one peak of the aerosol scattering coefficient is found in the early morning (about 379 Mm^{-1} for Sc and 48 Mm^{-1} for Bsp) and it is about 1-2 hours earlier than its absorption coefficient possibly owing to the different emissions between these two types of aerosols. Absorbing aerosols in urban Nanjing mainly come from the vehicle emissions because of the developed transportation network, resulting in two peaks of AAC within one day (Zhuang et al. 2015). Scattering aerosol loadings are somewhat less affected by traffic emissions especially in nighttime. Their precursors, such as SO_2 and NOx, mostly come from coal combustion and industrial emissions in urban Nanjing based on source apportionment. Therefore, there is no peak for SC or Bsp before midnight, although their values are considerably large (about 350 and 46 Mm^{-1}, respectively). Different diurnal cycles between AAC and SC were also observed in sub-urban area of Nanjing (Yu et al., 2016). Diurnal variations of AAC, SC and Bsp might be highly affected by the diurnal cycles of the boundary layer. The small coefficients in afternoon are mostly induced by well developed mixing layer (Zhuang et al. 2014b). Generally, the boundary layer becomes more and more stable after sunset and its height becomes lower, which is conducive to the accumulation of air pollutants in the nighttime especially during the period

from midnight to sunrise. Therefore, SC usually peaks in early morning and the peak appears at different times in different seasons (05:00 am in JJA and 08:00-09:00 am in DJF). The daytime peak of AAC appears at 07:00 am in JJA and at 09:00 am in DJF. Diurnal variation of SSA also reflects the difference between AAC and SC (Fig. 3d), implying that aerosols in urban Nanjing are more scattering after midnight (SSA is about 0.91) while more absorbing before noon and midnight (SSA is about 0.89). Scattering aerosols mainly come from strong chemical production (gas-to-particle transformation) at daytime, which to some extent might offset the dilution effect of the boundary on SC, thus, leading to a relatively larger SSA in afternoon. The figure further shows that both AAE (Fig. 3e) and SAE (Fig. 3f) at daytime are slightly larger than those after midnight because both absorbing and scattering aerosols are more fresher at daytime while they are more aged before sunrise. Diurnal variations of SAE and AAE are relatively weaker compared to corresponding coefficients. In addition to aerosol loadings, the level of Bsp is also affected by the size of the aerosols as suggested by Yu et al. (2016), so is ASP (Fig. 3g). Diurnal cycle of ASP is similar to that of Bsp but is opposite to that of SAE. Large ASP appears in early morning (0.587) and the lower ASP in afternoon (0.552).

Figure. 3

3.2 Frequencies of the aerosol optical properties

The frequency of the aerosol optical properties is presented in Figure 4 and Table 3. Similarly, the frequency of EC is not shown in the figure because it has similar pattern to SC's. Almost all of them follow a unimodal pattern. As listed in Table 3, the dominant ranges for all the aerosol optical properties are distributed around their annual mean values, respectively, with different widths and they account for at least 60% of the total samplings during the entire study period. The maximum frequencies of 32.9% (AAC), 24.04% (SC), 26.45% (Bsp), 18.64% (SSA), 20.9% (AAE), 18.06%

287 (SAE) and 34% (ASP) occur in the ranges from 9 to 21 Mm^{-1}, 170 to 280 Mm^{-1}, 30 to 45 Mm^{-1}, 0.91 to
288 93, 1.5 to 1.6, 1.32 to 1.5 and 0.55 to 0.62, respectively. Frequency distributions of the aerosol optical
289 properties have substantially seasonal variations. The frequency peaks of the properties would be more
290 concentrated at lower/higher ranges if their seasonal means are smaller/larger. As shown in Fig. 4a, 4c,
291 and 4e, relatively larger values or the peaks of frequencies for AAC, Bsp and AAE are concentrated in
292 lower value ranges in JJA but in higher value ranges in the other seasons. Moisture absorption growth
293 of absorbing aerosols leads to a left-ward shift in an AAE-frequency curve in JJA. Effects of dust
294 aerosol also might result in a left-ward shift in a SC-frequency curve in spring (Fig. 4f). Furthermore,
295 due to dust and RH, SC is considerably large in MAM and JJA, leading to relatively larger frequencies
296 of SC distributed at larger SC ranges compared with the ones of AAC. As mentioned above, aerosols in
297 urban Nanjing are more scattering and have stronger forward scattering ability in JJA than in the other
298 seasons, thus larger frequencies occur more at higher value ranges of SSA and ASP in JJA.

299 **Figure 4**

300 **Table 3**

301 **3.3 Aerosol optical properties in different wind directions**

302 East Asian monsoon is active in middle latitudes. Nanjing could be affected by East Asian summer
303 monsoon in JJA and by the winter monsoon in DJF. Air flows in these two seasons are significantly
304 different (Figure 5a and 5b) so to alter the aerosol optical properties in different seasons. Air masses
305 mostly come from the oceans (about 77%) in JJA and from continental regions in north and northwest
306 of China (57%) in DJF. Only a few percentages of air masses are from the north region of China in JJA.
307 Additionally, considerable air masses arriving at the site are from the local areas (cluster 1 in JJA) or
308 from places near Nanjing (cluster 1 in DJF). Therefore, the aerosol optical properties at the study site

309 are characterized differently with different air masses in the two seasons.

310 As suggested by Zhuang et al. (2014b), high BC loadings in early June 2012 were observed at the
311 site when the air masses were from northwestern directions of Nanjing, in which seriously biomass
312 burning was detected. Therefore, the aerosol optical properties are further analyzed by their origins in
313 both JJA and DJF (Fig 5c and 5d). In JJA, seasonal mean AAC, SC, Bsp, SSA, ASP, AAE and SAE are
314 about 19.65 Mm^{-1}, 340.87 Mm^{-1}, 36.99 Mm^{-1}, 0.93, 0.64, 1.49 and 1.34, respectively (Table 2). The
315 dominant air masses are from local areas (cluster 1 in Fig. a) and east ocean (on the way through urban
316 agglomeration regions (cluster 2) and less-developed regions (cluster 3) of the Yangtze River Delta
317 YRD), accounting for 90% of the total characteristics of the aerosol optical properties in urban Nanjing.
318 All the values of the properties in the first three clusters are more close to their season means. Aerosol
319 absorption and scattering coefficients from local emissions are larger than those in the other clusters.
320 Although air masses in cluster 2 and cluster 3 come from the oceans and have the same level of relative
321 humidity (RH), differences still exist between the clusters. The air masses have to cross the urban
322 agglomeration (from Shanghai to Nanjing) of YRD when they arrive Nanjing in cluster 2 but pass less
323 developed regions (north Jiangsu Province) in cluster 3. In YRD, emissions of the aerosols and trace
324 gases are much stronger in urban agglomeration regions than those in other area as suggested in Zhang
325 et al. (2009) and Zhuang et al. (2013b). Therefore, AAC and SC in cluster 2 are larger than those in
326 cluster 3 to some extent (Fig. 5a and 5c). Aerosols from these two clusters are more scattering than the
327 local ones. There are two clusters (cluster 4 and 5 in Fig. 5a) from the remote areas in JJA. Aerosol
328 loadings are relatively small when the air masses from these two clusters. The size of the aerosols is
329 finer (larger AAE in cluster 5 and SAE in cluster 4 and 5 in Fig. 5c). ASP varying with the clusters
330 coincides with RH varying with the clusters (Fig. 5c), implying that RH might influence ASP

significantly. In DJF, seasonal mean AAC, SC, Bsp, SSA, ASP, AAE and SAE are about 37.96 Mm^{-1}, 385.14 Mm^{-1}, 54.79 Mm^{-1}, 0.89, 0.54, 1.70 and 1.24, respectively (Table 2). Similar to JJA, the aerosol absorption and scattering coefficients are the largest, all of which (AAC, SC and Bsp) are about 1.3 times of their season means (Fig. 5d), when the air masses are local or from the regions (cluster 1 in Fig. 5b) near Nanjing in DJF. AAC, SC, Bsp, SSA and ASP are small but AAE and SAE are large if air masses are from remote areas. Aerosols are the smallest, most absorbing and finest when the air masses are from near Lake Baikal. ASP varying with the clusters also coincides with RH varying with the clusters in this season (Fig. 5d), further implying the effect of RH on ASP.

Figure 5

Substantial studies on the aerosol optical properties have been carried out in China from monthly to annual scales. Table 4 lists some annual and seasonal statistics of measured surface aerosol optical properties from literature. Annual and season means listed in the table are comparable to some extent, although the observational periods and instruments are different. It suggests that AACs and SCs in urban areas are much higher than those in rural and remote areas. In Beijing (center of Beijing-Tianjin-Hebei region), annual mean AAC and SC were 56 and 288 Mm^{-1} in urban site during the period from 2005 to 2006 (He et al., 2009), which were much larger than the ones (17.5 and 174.6 Mm^{-1}, respectively) in rural area (Yan et al., 2008). In Chengdu (Tao et al., 2014), Xi'an (Cao et al., 2012) and Wuhan (Gong et al., 2015), which is the center from southwest to central China, the annual mean scattering coefficients in these cities exceeded 450, 520 and 370 Mm^{-1}, respectively. In Pearl River Delta (PRD) region, seasonal mean AAC at 532 nm was about 84 and 188 Mm^{-1} at an urban site (Panyu), about 47 and 95 Mm^{-1} at a suburban site (Dongguan), about 26 and 28 Mm^{-1} at a rural site, and only 7.21 and 8.37 Mm^{-1} at a remote site (Yongxing Island), in spring and winter, respectively (Wu

et al., 2013). Additionally, aerosols in urban areas are more absorbing. The aerosol absorptions in urban areas have stronger seasonality than those in rural areas (Table 4). Urban aerosols in Nanjing in annual scale are somewhat lower but more scattering than those in most cities in China. In addition to annual and seasonal means, there are considerable studies on monthly mean aerosol optical properties (e.g., Bergin et al., 2001; Xu et al., 2002; 2004; Li et al., 2007; Andreae et al., 2008; Li et al., 2015a; b). A few studies on the aerosol optical properties in Nanjing have been carried out previously (Zhuang et al., 2014a; 2015; Yu et al., 2016) based on observations. They were more focused on the columnar aerosols (Zhuang et al., 2014a), or single optical property (Zhuang et al., 2015), or shorten observations (two months in Yu et al., 2016). Substantial analysis in the key optical properties of the surface aerosol here to a certain degree fill the gaps in the study on the aerosols in Nanjing, even in YRD.

Table 4

3.4 Relationship among aerosol optical properties, relative humidity and visibility

The relationships between SC and AAC, SC and Bsp are presented by season in Figure 6. As shown in Figures 3 and 4, these three types of coefficients have similar diurnal and frequency distributions. The linear correlation coefficient varies from 0.93 to 0.97 for SC and Bsp and from 0.66 to 0.87 for SC and AAC in urban Nanjing. It is obvious that relations between SC and Bsp are much better than those between SC and AAC in all seasons. The correlation between AAC and SC becomes poorer in MAM (0.66) and JJA (0.78) because the scattering aerosols is more affected by dust in spring and SC is more affected by RH in summer. The linear correlation coefficients between SC and AAC and between SC and Bsp in MAM at the site were a little smaller than that in suburban Nanjing (Yu et al., 2016) in the same season in 2011. The slope of the fitting between Bsp and SC represents the levels of ASP. Analysis (not shown) suggests that ASP has a significant anti-correlation with the ratio of Bsp

375 to SC (linear R=-0.98). Thus, a greater slope of curve represents a smaller ASP, thus less forward
376 scattering of the aerosols.

377 **Figure 6**

378 The correlations between ASP and SC under different RH conditions are illustrated in Figure 7,
379 showing that ASP has a quasi-LogNormal distribution with SC especially in lower RH conditions. ASP
380 increases monotonically with increasing SC in low RH ranges (Fig. 7a and 7b, RH < 60%) and ASP
381 mostly concentrates at small SC regions when RH is less than 40% (Fig. 7a), implying that fine
382 particles dominates the most in low RH conditions as also suggested by Andrews et al. (2006) and
383 Badu et al. (2012). The correlation between ASP and SC becomes poorer with increasing RH (Fig. c),
384 indicating that both fine and coarse aerosols might be equally important to the total SC.

385 **Figure 7**

386 Figure 8 shows the relationships between the SSA at 491 nm and extinction Angstrom exponent
387 (EAE) at 491/863 nm (Fig. a) as well as between SSA difference (863 nm - 491 nm) (short for dSSA)
388 and EAE at 491/863 nm (Fig. b). Overall, SSA or dSSA to a certain degree have an anti-correlation
389 with EAE in urban area of Nanjing, especially for the latter one. Linear correlation coefficient is about
390 -0.13 between SSA and EAE and about -0.75 between dSSA and EAE. Relationships between the SSA
391 (or dSSA) and EAE to some extent reflect the aerosol types and sources as indicated by Russell et al.
392 (2014), who proposed a method to identify the aerosol types based on the columnar aerosol optical
393 properties (including SSA, EAE and the real refractive index) from the Aerosol Robotic Network
394 (AERONET) retrievals. They suggested that: 1. The polluted dust aerosol had smaller EAE (near 1.0)
395 and SSA ranged from 0.85 to 0.95. 2. The urban aerosols had larger EAE values (around 1.4) and SSA
396 ranges (0.86~1.0) compared with the dust aerosols. 3. The biomass burning aerosol (dark type) had the

largest EAE (exceeding 1.5) while smaller SSA (about 0.85). If there were two kind of aerosols having nearly identical coordinates in SSA and EAE, further information (such as the real refractive index) should be used (Russell et al., 2014). Based on this method, the figure further implies that, in addition to local emissions, aerosols in urban area of Nanjing might also be affected substantially by the long distance transported dust (or polluted dust) in spring and be influenced to some extent by biomass burning in fall.

Figure 8

Atmospheric humidity has significant influences on the growth of particulate matter, subsequently affecting the sizes and absorbing/scattering abilities of the aerosols. As shown in Figure 7a and 7c, high levels of SC are likely found in high RH ranges. Seasonal mean RH is the largest in summer but lowest in winter (Figure 9a). In summer, both trace gases and particulate matters have lower emission rates as suggested by Zhang et al. (2009). Furthermore, PBL height and precipitation mostly have larger values in this season than those in other seasons. Thus, these three factors would result in smaller aerosol loadings in summer. However, different from Bsp, SC in summer is larger than that in spring and fall possibly due to the effects of RH (Fig. 1c and 1d). Zhang et al. (2015) indicated that SC and Bsp in YRD would increase by 50% and 25% as the RH increased from 40% to 85% and the increment would become larger if there were considerable amount of nitrate in fine particles. And nitrate in urban area of Nanjing accounts for more than 20% (as much as sulfate) of the total PM2.1 (Zhuang et al., 2014a). RH might also affect the sizes of the aerosol. The smallest AAE in JJA always corresponds to the highest RH, and vice versa (Fig. 1b and 9a). These results are consistent with Zhuang et al. (2014a), in which characteristic of columnar aerosol optical properties were investigated. Figure 9b further shows that AAE and SAE decrease monotonically with increasing RH. The correlation between ASP and RH is

opposite to that between aerosol Ångström exponent and RH, further implying that the forward scattering efficiency increases with increasing in RH. The linear correlation coefficients are -0.36, -0.15 and 0.6 between AAE and RH, SAE and RH, and ASP and RH, respectively, in urban areas of Nanjing. The relation between ASP and RH is the best among these three optical properties, which has somewhat shown in Fig. 2f, Fig. 5c and Fig. 5d. These results could be used to correct the aerosol optical parameters in numerical models for estimating the aerosol radiative forcing in East China as suggested by Andrews et al. (2006), in hope to reduce uncertainties in such estimation.

Figure 9

High levels of aerosol loadings would directly affect the visibility (VIS), which is one of the factors being concerned about in current air quality forecasting in China. The forecast accuracy of visibility or haze pollutions would be increased significantly if the effects of aerosols on visibility can be figured out. Instead of the loadings of the particulate matter, the aerosol optical properties here are used when investigating the aerosol effects on VIS.

Figure 10 shows the relations between extinction coefficient (EC) and VIS and between SC and VIS by season under different RH levels. Atmospheric VIS is found to decrease exponentially with increasing EC or SC in all seasons. The lapse rate of VIS with EC or SC is much larger in spring and summer than in fall and winter. The lower VIS always appears at higher RH ranges, and vice versa. In small VIS regions (such as: <4 km), VIS values are much smaller in JJA than those in the other seasons under the same SC level, implying the strong effects of RH on VIS. The effect of AAC on VIS has substantial seasonality and it is strong in SON but weak in MAM and JJA as illustrated in the fitting lines in the figure. Study on the effects of PM on VIS might be more reasonable if using the aerosol optical properties rather than its mass concentrations. The linear correlation coefficient between EC and

441 VIS varies from -0.69 (in JJA) to -0.87 (in DJF), and between SC and VIS, it varies from -0.71 (in JJA)
442 to -0.87 (in DJF) in urban area of Nanjing.

443 **Figure 10**

444 In addition to the SC or EC, the aerosol SSA and ASP also have good relationships with VIS as
445 shown in Figure 11, in which the effects of RH and SAE are also included (larger markers represent
446 smaller SAE, but larger size of the aerosols). The aerosols become coarser, less absorbing and more
447 forward scattering with increasing RH, which subsequently further exacerbate the deterioration of
448 visibility in all the seasons. The linear correlation coefficients vary from -0.48 (in JJA) to -0.73 (in
449 SON) between SSA and VIS and -0.47 (in JJA) to -0.80 (in MAM) between ASP and VIS in urban
450 Nanjing. These results additionally illustrate that the scattering aerosols are still the key factors
451 affecting the atmospheric visibility, although the absorbing aerosols might have considerable influences
452 on VIS in some seasons (Fig. 10c). The results in this study further indicate that effects of aerosols on
453 air quality are complex.

454 **Figure 11**

455 Comparison between surface aerosol extinction coefficient and columnar AOD is performed
456 (Figure 12). Differences exist between EC and AOD, although they are well correlated with each other
457 in each season. AOD to some extent is less affected by the development of boundary layer and more
458 affected by the transport of aerosols compared to EC at the surface. The seasonal mean EC is large both
459 in JJA and in DJF while the largest AOD is only found in JJA, which is possibly related to higher
460 boundary layer height in JJA. A lower boundary layer would lead to more aerosol accumulation at the
461 surface thus result in its smaller column burden. These differences (high surface aerosol loadings but
462 low AOD) have also been simulated by a regional climate chemistry model in Zhuang et al. (2011 and

2013). Overall, high AOD level corresponds to large EC value in each season, implying that aerosols in the upper layers mostly come from surface emissions in urban Nanjing. In some cases, long distance transport of aerosols might contributes significantly to the AOD as shown in Fig. 12a, in which AOD exceeds 2 meanwhile EC is found to appear in low value ranges. The slope of the linear fitting is larger in JJA (about 0.0016) than that in the other seasons (all about 0.001), indicating that for a given value of EC, AOD would be higher in JJA possibly because of higher humidity in summer. The columnar water vapor in summer is about 2 to 5 times of that in the other seasons.

Figure 12

4 Conclusions

In this study, the near-surface aerosol optical properties, including aerosol scattering (SC), back scattering (Bsp), absorption (AAC) and extinction (EC) coefficients, single scattering albedo (SSA), scattering (SAE) and absorbing (AAE) Ångström exponent, as well as asymmetry parameter (ASP), are investigated based on the measurements with the 7-channel Aethalometer (model AE-31, Magee Scientific, USA) and three-wavelength integrating Nephelometer (Aurora 3000, Australia) in urban area of Nanjing.

In urban area of Nanjing, the annual mean EC, SSA and ASP at 550 nm are 381.958 Mm^{-1}, 0.901, 0.571, respectively. SC, which accounts for about 90% of EC, is about one order of magnitude larger than AAC, implying that EC to a great degree has similar temporal variation and frequency distribution to SC. Absorbing aerosol is finer than the scattering one. AAE at 470/660 nm is about 1.58, about 0.2 larger than SAE. All of them above have substantially seasonal and diurnal variations. Both the aerosol absorption and scattering coefficients have the largest values in winter due to the higher emissions. However, SC also has a higher values in summer and spring likely due to higher relative humidity (RH)

485 and efficiency of gas-to-particle transformation in summer and the effect of dust in spring, respectively.
486 High RH in summer results in the lowest AAE and largest ASP being found and it is also lead to a
487 relatively smaller SAE, although a large number of fine scattering aerosols could be produced through
488 intensive gas-to-particle transformation in this season. Seasonality of SSA is co-determined by AAC
489 and SC, showing the largest value in summer and lowest value in fall. AAC, SC, Bsp and EC have
490 more substantial diurnal variations than SSA, AAE, SAE and ASP. Because of traffic emissions, AACs
491 are high at the rush hours (around 09:00 am and pm) but low in afternoon when the boundary layer
492 being well developed. SC and Bsp usually peak in the early morning before sunrise (1-2 earlier than
493 AAC's) and reach the bottom in the afternoon. High levels of SC and Bsp are mostly caused by
494 accumulation of air pollution in the nighttime from midnight to sunrise. The diurnal variation of SSA is
495 also depended on AAC and SC. SSA is large after midnight and noon. AAE and SAE at daytime are
496 slightly larger than after midnight because both absorbing and scattering aerosols are fresher at daytime
497 but more aged before sunrise. ASP, which is related to the size of the aerosols, its diurnal variation is
498 opposite to SAE's but similar to Bsp's.

499 The seasonal and diurnal observations on the aerosol optical properties are of great importance to
500 the modeling community. In addition to the aerosol emission rates, compositions, mixing states, and
501 profiles, uncertainties of the aerosol seasonality and diurnal variations might also lead to large bias
502 when investigating the aerosol radiative forcing and climate effects. Xu et al. (2016) presented that the
503 aerosol direct radiative forcing would be underestimated both at the TOA and surface by 2.0 and 38.8
504 W/m^2, respectively, if the diurnal variation were excluded. Large bias of the aerosol forcing would
505 subsequently result in substantial uncertainties of the climate responses to the aerosol. Analysis on the
506 seasonal and diurnal variations of the aerosol optical properties in this study to some extent are

507 valuable to the modeling-based researches on the aerosol climate effects.

508 Frequency analysis indicates that almost all of the aerosol optical properties follow a unimodal
509 pattern in urban area of Nanjing. The ranges around their averages, with different widths, accounting
510 for more than 60% of the total samplings. Frequency distributions of the aerosol optical properties also
511 have substantial seasonality. The frequency peak of a property would be more concentrated among
512 lower/higher ranges if the seasonal mean is smaller/larger. Back trajectory analysis suggests that the
513 source of aerosols in Nanjing are mainly from the local and regional emissions around YRD in summer,
514 while from the sources include both local emissions and transport from central and north China in
515 winter. In JJA, aerosols are more scattering when air masses come from the East China Sea and finer if
516 air masses come from remote areas. In DJF, AAC, SC, Bsp, SSA and ASP are low while AAE and SAE
517 are high in urban Nanjing under the conditions of air masses being transported from remote areas. ASP
518 varied with the clusters is consistent with RH in both JJA and DJF.

519 The correlation between SC and Bsp is much better than that between SC and AAC in all seasons.
520 In spring, these relationships are a little weaker than those in suburban Nanjing. ASP has a
521 quasi-LogNormal distribution with SC under a condition of RH being lower than 60%, increasing
522 monotonically with increasing SC. It would be mostly concentrated at small SC regions when RH is
523 less than 40% because finer particles dominant under low RH conditions. The correlation between ASP
524 and SC becomes weaker with increasing RH, indicating that both fine and coarse aerosols might be
525 equally important to the total SC in high RH conditions. Atmospheric humidity can significantly
526 modulate aerosol optical properties. Due to the effects of RH in summer, the aerosol would become
527 coarser and its forward scattering efficiency would be stronger with increasing in RH. The linear
528 correlation coefficients are -0.36, -0.15 and 0.6 between AAE and RH, SAE and RH, and ASP and RH,

529 respectively, in urban areas of Nanjing. Comparisons also indicate that seasonal variation of surface
530 aerosol EC (high in JJA and DJF) is different from its columnar optical depth (AOD, high in JJA and
531 low in DJF), even though they are closely correlated to each other within each season. Overall, high
532 AOD level corresponding to large EC value in each season implies that aerosols in upper layers are
533 mostly from surface emissions. AOD would be higher in JJA than in other seasons in a condition with
534 fixed EC, possibly due to the effects of high humidity.

535 Overall, the scattering aerosols are still the key factor in affecting the atmospheric visibility
536 (VIS), although the absorbing aerosol has considerable contributions in some seasons. The linear
537 correlation coefficient between EC and VIS varies from -0.69 to -0.87, close to those between SC and
538 VIS. VIS is found to be decreased exponentially with increasing EC or SC in all seasons. And its lapse
539 rate along with EC or SC is much larger in spring and summer than in fall and winter. In small VIS
540 regions (i.e., VIS<4 km), VIS values are much smaller in JJA than in other seasons if the SC levels are
541 the same, further indicating the strong effect of RH on VIS. The aerosol SSA and ASP could also affect
542 VIS. Large SSA and ASP might further exacerbate the deterioration of visibility. The linear correlation
543 coefficients between seasonal SSA and VIS varies from -0.48 to -0.73 and from -0.47 to -0.80 between
544 ASP and VIS in urban area of Nanjing.

545

546 **Acknowledgements:** This work was supported by the National Key Basic Research Development
547 Program of China (2014CB441203), the National Natural Science Foundation of China (41675143,
548 91544230, 41621005), the New Teachers' Fund for Postdoctoral Fellows, Ministry of Education
549 (20120091120031), FP7 project: REQUA (PIRSES-GA-2013-612671), and a project Funded by the
550 Priority Academic Program Development of the Jiangsu Higher Education Institutions (PAPD). the

551 National Science Foundation of Jiangsu Provence (Grant #BE2015151). The authors would like to
552 thank all members in the AERC of Nanjing University for maintaining instruments. The HYSPLIT
553 model was supplied by NOAA: http://ready.arl.noaa.gov/HYSPLIT_traj.php.

554 **5 References**

555 Andreae, M. O., Schmid, O., Yang, H., Chand, D., Yu, J. Z., Zeng, L. M., and Zhang, Y. H.: Optical
556 properties and chemical composition of the atmospheric aerosol in urban Guangzhou, China Atmos.
557 Environ., 42, 6335–6350, 2008.

558 Andrews, E., Sheridan, P. J., Fiebig, M., McComiskey, M., Ogren, J. A., Arnott, P., Covert, D., Elleman,
559 R., Gasparini, R., Collins, D., Jonsson, H., Schmid, B., and Wang, J.: Comparison of methods for
560 deriving aerosol asymmetry parameter, J. Geophys. Res., 111, D05S04, doi:10.1029/2004JD005734,
561 2006.

562 Arnott, W. P., Hamasha, K., Moosmuller, H., Sheridan, P. J., and Ogren, J. A.: Towards aerosol
563 light-absorption measurements with a 7-wavelength aethalometer: evaluation with a photoacoustic
564 instrument and 3-wavelength nephelometer, Aerosol Sci. Tech., 39, 17–29,
565 doi:10.1080/027868290901972, 2005.

566 Babu, S., Gogoi, M., Kumar, V. H. A., Nair, V. S., Moorthy, K. K.: Radiative properties of Bay of
567 Bengal aerosols: spatial distinctiveness and source impacts, J. Geophys. Res., 117, D06213,
568 doi:10.1029/2011JD017355, 2012.

569 Bai, H. T., Chen, Y. H., Wang, H. Q., Zhang, Q., Guo, N., Wang, S., Pan, H., and Zhang, P.: Seasonal
570 variation of aerosol optical properties at AERONET of the semi-arid region in Loess Plateau, Arid
571 Land Geogr., 34, 1–8, 2011.

572 Bellouin, N., Boucher, O., Tanré, D., and Dubovik, O.: Aerosol absorption over the clear-sky oceans
573 deduced from POLDER-1 and AERONET observations, Geophys. Res. Lett., 30, 1748,
574 doi:10.1029/2003GL017121, 2003.

575 Bergin, M. H., Cass, G. R., Xu, J., Fang, C., Zeng, L., Yu, T., Salmon, L. G., Kiang, C. S., Tang, X. Y.,

576 Zhang, Y. H., and Chameides, W. L.: Aerosol radiative, physical, and chemical properties in Beijing
577 during June 1999, J. Geophys. Res., 106 (D16), 17969–17980, 2001.
578 Cai, H. K., Zhou, R. J., Fu, Y. F., Zheng, Y. Y., and Wang, Y. J.: Cloud-aerosol lidar with or thogonal
579 polarization detection of aerosol optical properties after a crop burning case, Clim. Environ. Res.,
580 16, 469–478, 2011.
581 Cao, J., Wang, Q., Chow, J. C., Watson, J. G., Tie, X., Shen, Z., Wang, P., and An Z.: Impacts of aerosol
582 compositions on visibility impairment in Xi'an, China, Atmos. Environ., 59, 559–566, 2012.
583 Chameides, W. L., and Bergin, M.: Soot takes center stage, Science, 297 (5590), 2214-2215, 2002.
584 Che, H. Z., Zhang, X. Y., Xia, X., Goloub, P., Holben, B., Zhao, H., Wang, Y., Zhang, X. C., Wang, H.,
585 Blarel, L., Damiri, B., Zhang, R., Deng, X., Ma, Y., Wang, T., Geng, F., Qi, B., Zhu, J., Yu, J., Chen,
586 Q., and Shi, G..: Ground-based aerosol climatology of China: aerosol optical depths from the China
587 Aerosol Remote Sensing Network (CARSNET) 2002–2013, Atmos. Chem. Phys., 15, 7619–7652,
588 2015.
589 Cheng, Y. F., Wiedensohler, A., Eichler, H., Su, H., Gnauk, T., Bruggemann, E., Herrmann, H.,
590 Heintzenberg, J., Slanina, J., Tuch, T., Hu, M., and Zhang, Y. H.: Aerosol optical properties and
591 related chemical apportionment at Xinken in Pearl River Delta of China, Atmos. Environ., 42,
592 6351–6372, 2008.
593 Collaud Coen, M., Weingartner, E., Apituley, A., Ceburnis, D., Fierz-Schmidhauser, R., Flentje, H.,
594 Henzing, J. S., Jennings, S. G., Moerman, M., Petzold, A., Schmid, O., and Baltensperger, U.:
595 Minimizing light absorption measurement artifacts of the Aethalometer: evaluation of five
596 correction algorithms, Atmos. Meas. Tech., 3, 457–474, doi:10.5194/amt-3-457-2010, 2010.
597 Fan, X. H., Chen, H. B., Xia, X. A., Li, Z. Q., and Cribb, M.: Aerosol optical properties from the

598 Atmospheric Radiation Measurement Mobile Facility at Shouxian. China, J. Geophys. Res., 115,
599 D00K33, doi:10.1029/2010JD014650, 2010.
600 Forster, P., Ramaswamy, V., Artaxo, P., Berntsen, T., Betts, R., Fahey, D. W., Haywood, J., Lean, J.,
601 Lowe, D. C., Myhre, G., Nganga, J., Prinn, R., Raga, G., Schulz, M., and Van Dorland, R.: Changes
602 in atmospheric constituents and in radiative forcing, in: Climate Change 2007: The Physical
603 Science Basis. Contribution of Working Group I to the Fourth Assessment Report of the
604 Intergovernmental Panel on Climate Change, edited by: Solomon, S. et al., Cambridge Univ. Press,
605 Cambridge, UK, 129–234, 2007.
606 Gong, W., Zhang, M., Han, G., Ma, X., and Zhu, Z.: An investigation of aerosol scattering and
607 absorption properties in Wuhan, Central China, Atmosphere, 6, 503–520, 2015.
608 Guo, J., Miao, Y., Zhang, Y., Liu, H., Li, Z., Zhang, W., He, J., Lou, M., Yan, Y., Bian, L., and Zhai,
609 P.: The climatology of planetary boundary layer height in China derived from radiosonde and
610 reanalysis data, Atmos. Chem. Phys. Discuss., doi:10.5194/acp-2016-564, 2016b.
611 Guo, J., M. Deng, S. S. Lee, F. Wang, Z. Li, P. Zhai, H. Liu, W. Lv, W. Yao, and X. Li: Delaying
612 precipitation and lightning by air pollution over the Pearl River Delta. Part I: Observational
613 analyses, J. Geophys. Res. Atmos., 121, 6472–6488, doi:10.1002/2015JD023257.2016a.
614 Guo, J.P., X. Zhang, H. Che, S. Gong, X. An, C.X. Cao, J. Guang, H. Zhang, Y.Q. Wang, X.C. Zhang,
615 P. Zhao, X.W. Li: Correlation between PM Concentrations and Aerosol Optical Depth in Eastern
616 China, Atmospheric Environment, 43(37): 5876-5886. 2009.
617 He, X., Li, C. C., Lau, A. K. H., Deng, Z. Z., Mao, J. T., Wang, M. H., and Liu, X. Y.: An intensive
618 study of aerosol optical properties in Beijing urban area, Atmos. Chem. Phys., 9, 8903–8915,
619 doi:10.5194/acp-9-8903-2009, 2009.

620 Holler, R., Ito, K., Tohno, S., and Kasahara, M.: Wavelength-dependent aerosol single scattering albedo:
621 measurements and model calculations for a coastal site near the sea of Japan during ACE-Asia, J.
622 Geophys. Res., 108, 8648, doi:10.1029/2002JD003250, 2003.
623 IPCC, 2013: Climate Change 2013: The Physical Science Basis. Contribution of Working Group I to
624 the Fifth Assessment Report of the Intergovernmental Panel on Climate Change [Stocker, T.F., D.
625 Qin, G.-K. Plattner, M. Tignor, S.K. Allen, J. Boschung, A. Nauels, Y. Xia, V. Bex and P.M.
626 Midgley (eds.)]. Cambridge University Press, Cambridge, United Kingdom and New York, NY,
627 USA, 1535 pp.
628 Jacobson, M. Z.: Control of fossil-fuel particulate black carbon and organic matter, possibly the most
629 effective method of slowing global warming, J. Geophys. Res., 107, 4410,
630 doi:10.1029/2001JD001376, 2002.
631 Kiehl, J. T. and Briegleb, B. P.: The relative roles of sulfate aerosols and greenhouse gases in climate
632 forcing, Science, 260, 311–314, 1993.
633 Li, C., Marufu, L. T., Dickerson, R. R., Li, Z., Wen, T., Wang, Y., Wang, P., Chen, H., and Stehr, J. W.:
634 In situ measurements of trace gases and aerosol optical properties at a rural site in northern China
635 during East Asian Study of Tropospheric Aerosols: An International Regional Experiment 2005, J.
636 Geophys. Res., 112, D22S04, doi:10.1029/2006JD007592, 2007.
637 Li, J., Liu, X., Yuan, L., Yin, Y., Li, Z., Li, P., Ren, G., Jin, L., Li, R., Dong, Z., Li, Y., and Yang, J.:
638 Vertical distribution of aerosol optical properties based on aircraft measurements over the Loess
639 Plateau in China, J. Environ. Sci, 34, 44-56, 2015a.
640 Li, J., Yin, Y., Li, P., Li, Z., Li, R., Cribb, M., Dong, Z., Zhang, F., Li, J., Ren, G., Jin, L., and Li, Y.:
641 Aircraft measurements of the vertical distribution and activation property of aerosol particles over

the Loess Plateau in China, Atmos. Res., 155, 73–86, 2015b.

Li, Z., C. Li, H. Chen, et al.: East Asian Studies of Tropospheric Aerosols and their Impact on Regional Climate (EAST-AIRC): An overview. J. Geophys. Res. 116, D7, doi:10.1029/2010jd015257.2011.

Li, Z. Q., Lee, K. H., Wang, Y. S., Xin, J. Y., and Hao, W. M.: First observation-based estimates of cloud-free aerosol radiative forcing across China, J. Geophys. Res., 115, D00K18, doi:10.1029/2009JD013306, 2010.

Liao, H. and Seinfeld, J. H.: Global impacts of gas-phase chemistry-aerosol interactions on direct radiative forcing by anthropogenic aerosols and ozone, J. Geophys. Res., 110, D18208, doi:10.1029/2005JD005907, 2005.

Menon, S., Hansen, J., Nazarenko, L., and Luo, Y. F.: Climate effects of black carbon aerosols in China and India, Science, 297, 2250–2253, doi:10.1126/science.1075159, 2002.

Penner, J. E., Andreae, M., Annegarn, H., Barrie, L., Feichter, J., Hegg, D., Jayaraman, A., Leaitch, R., Murphy, D., Nganga, J., and Pitari, G.: Aerosols, their direct and indirect effects, in: Climate Change 2001: The Scientific Basis. Contribution of Working Group I to the Third Assessment Report of the Intergovernmental Panel on Climate Change, edited by: Houghton, J. T. et al., Cambridge University Press, Cambridge, UK and New York, NY, USA, 289–348, 2001.

Petzold, A., Kopp, C., and Niessner, R.: The dependence of the specific attenuation cross-section on black carbon mass fraction and particle size, Atmos. Environ., 31, 661–672, 1997.

Qian, Y., Gong, D.Y., Fan, J.W., Leung, L.R., Bennartz, R., Chen, D.L., Wang, W.G.: Heavy pollution suppresses light rain in China: Observations and modeling. J. Geophys. Res. 114, D00K02, doi:10.1029/2008jd011575. 2009.

Qin, S. G., Tang J, Wen YP (2001) Black carbon and its importance in climate change studies.

664 Meteorol Monogr 27(11):3–7.

665 Rosenfeld, D., Lohmann, U., Raga, G.B., O'Dowd, C.D., Kulmala, M., Fuzzi, S., Reissell, A., Andreae,

666 M.O.: Flood or drought: how do aerosols affect precipitation? Science 321, 5894, 1309-1313.

667 2008.Russell, P. B., Kacenelenbogen, M., Livingston, J. M., Hasekamp, O. P., Burton, S. P.,

668 Schuster, G. L., Johnson, M. S., Knobelspiesse, K. D., Redemann, J., Ramachandran, S., and

669 Holben, B.: A multiparameter aerosol classification method and its application to retrievals from

670 spaceborne polarimetry, J. Geophys. Res. Atmos., 119, 9838–9863, doi:10.1002/2013JD021411,

671 2014.

672 Schmid, O., Artaxo, P., Arnott, W. P., Chand, D., Gatti, L. V., Frank, G. P., Hoffer, A., Schnaiter, M., and

673 Andreae, M. O.: Spectral light absorption by ambient aerosols influenced by biomass burning in the

674 Amazon Basin. I: Comparison and field calibration of absorption measurement techniques, Atmos.

675 Chem. Phys., 6, 3443–3462, doi:10.5194/acp-6-3443-2006, 2006.

676 Streets, D. G., Gupta, S., Waldhoff, S. T., Wang, M. Q., Bond, T. C., and Bo, Y. Y.: Black carbon

677 emissions in China, Atmos. Environ., 35, 4281–4296, doi:10.1016/S1352-2310(01)00179-0, 2001.

678 Tao, J., Zhang, L. M., Cao, J. J., Hsu, S. C., Xia, X. G., Zhang, Z. S., Lin, Z. J., Cheng, T. T., and Zhang,

679 R. J.: Characterization and source apportionment of aerosol light extinction in Chengdu, southwest

680 China, Atmos. Environ., 95, 552–562, 2014.

681 Wang, T. J., Zhuang, B. L., Li, S., Liu, J., Xie, M., Yin, C. Q., Zhang, Y., Yuan, C., Zhu, J. L., Ji, L. Q.,

682 and Han, Y.: The interactions between anthropogenic aerosols and the East Asian summer monsoon

683 using RegCCMS, J. Geophys. Res. Atmos., 120, doi:10.1002/2014JD022877, 2015.

684 Wang, Y., Che, H. Z., Ma, J. Z., Wang, Q., Shi, G. Y., Chen, H. B., Goloub, P., and Hao, X. J.: Aerosol

685 radiative forcing under clear, hazy, foggy, and dusty weather conditions over Beijing, China,

686 Geophys. Res. Lett., 36, L06804, doi:10.1029/2009GL037181, 2009.
687 Wang, Y., Wang, M., Zhang, R., et al., 2014. Assessing the effects of anthropogenic aerosols on
688 Pacific storm track using a multiscale global climate model. Proceedings of the National Academy
689 of Sciences 111, 19, 6894-6899.
690 Weingartner, E., Saathoff, H., Schnaiter, M., Streit, N., Bitnar, B., and Baltensperger, U.: Absorption of
691 light by soot particles: determination of the absorption coefficient by means of aethalometers, J.
692 Aerosol Sci., 34, 1445–1463, doi:10.1016/S0021-8502(03)00359-8, 2003.
693 Wu, D., Mao, J. T., Deng, X. J., Tie, X. X., Zhang, Y. H., Zeng, L. M., Li, F., Tan, H. B., Bi, X. Y.,
694 Huang, X. Y., Chen, J., and Deng, T.: Black carbon aerosols and their radiative properties in the
695 Pearl River Delta region, Sci. China Ser. D, 52, 1152–1163, doi:10.1007/s11430-009-0115-y, 2009.
696 Wu, D.,Wu, C., Liao, B., Chen, H.,Wu, M., Li, F., Tan, H., Deng, T., Li, H., Jiang, D., and Yu, J. Z.:
697 Black carbon over the South China Sea and in various continental locations in South China, Atmos.
698 Chem. Phys., 13, 12257–12270, doi:10.5194/acp-13-12257-2013, 2013.
699 Wu, Y. F., Zhang, R. J., Pu, Y. F., Zhang, L. M., Ho, K. F., and Fu, C. B.: Aerosol optical properties
700 observed at a semi-arid rural site in northeastern China, Aerosol Air Qual. Res., 12, 503–514, 2012.
701 Xia, X. A., Li, Z. Q., Holben, B., Wang, P., Eck, T., Chen, H. B., Cribb, M., and Zhao, Y. X.: Aerosol
702 optical properties and radiative effects in the Yangtze Delta region of China, J. Geophys. Res., 112,
703 D22S12, doi:10.1029/2007JD008859, 2007.
704 Xiao, Z. Y., Jiang, H., Chen, J., Wang, B., and Jiang, Z. S.: Monitoring the aerosol optical properties
705 over Hangzhou using remote sensing data, Acta Sci. Circumst., 31, 1758–1767, 2011.
706 Xin, J., Wang, Y., Pan, Y., et al.: The Campaign on Atmospheric Aerosol Research Network of China:
707 CARE-China. Bulletin of the American Meteorological Society 96, 7, 1137-1155,

doi:10.1175/BAMS-D-14-00039.1. 2014.

Xu, J., Bergin, M. H., Greenwald, R., Schauer, J. J., Shafer, M. M., Jaffrezo, J. L., and Aymoz, G.: Aerosol chemical, physical, and radiative characteristics near a desert source region of Northwest China during ACE-Asia, J. Geophys. Res., 109, D19S03, doi:10.1029/2003JD004239, 2004.

Xu, J., Bergin, M. H., Yu, X., Liu, G., Zhao, J., Carrico, C. M., and Baumann, K.: Measurement of aerosol chemical, physical and radiative properties in the Yangtze delta region of China, Atmos. Environ., 36, 161–173, 2002.

Xu, J., Tao, J., Zhang, R., Cheng, T., Leng, C., Chen, J., Huang, G., Li, X., and Zhu, Z.: Measurements of surface aerosol optical properties in winter of Shanghai, Atmos. Res., 109-110, 25–35, 2012.

Yan, P., Tang, J., Huang, J., Mao, J. T., Zhou, X.J., Liu, Q., Wang, Z. F., and Zhou, H. G.: The measurement of aerosol optical properties at a rural site in Northern China, Atmos. Chem. Phys., 8, 2229–2242, doi:10.5194/acp-8-2229-2008, 2008.

Yan, P.: Study on the aerosol optical properties in the background regions in the East part of China, PhD Thesis, Peking University, China, 2006.

Yu, X. N., Ma, J., Kumar, K. R., Zhu, B., An, J. L., He, J. Q., and Li, M.: Measurement and analysis of surface aerosol optical properties over urban Nanjing in the Chinese Yangtze River Delta, Sci. Total Environ., 542, 277-291, 2016.

Zhang, L., Sun, J. Y., Shen, X. J., Zhang, Y. M., Che, H., Ma, L. Q., Zhang, Y. W., Zhang, X. Y., and Ogren, J. A.: Observations of relative humidity effects on aerosol light scattering in the Yangtze River Delta of China, Atmos. Chem. Phys., 15, 8439–8454, 2015.

Zhang, Q., Streets, D. G., Carmichael, G. R., He, K. B., Huo, H., Kannari, A., Klimont, Z., Park, I. S., Reddy, S., Fu, J. S., Chen, D., Duan, L., Lei, Y., Wang, L. T., and Yao, Z. L.: Asian emissions in

2006 for the NASA INTEX-B mission, Atmos. Chem. Phys., 9, 5131–5153, doi:10.5194/acp-9-5131-2009, 2009.

Zhang, W., Hu, B., Chen, C. H., Du, P., Zhang, L., and Feng, G. H.: Scattering properties of atmospheric aerosols over Lanzhou City and applications using an integrating nephelometer, Adv. Atmos. Sci., 21(6), 848–856, 2004.

Zhang, X. Y., Wang, Y. Q., Niu, T., Zhang, X. C., Gong, S. L., Zhang, Y. M., and Sun, J. Y.: Atmospheric aerosol compositions in China: Spatial/temporal variability, chemical signature, regional haze distribution and comparisons with global aerosols, Atmos. Chem. Phys., 12, 779–799, doi:10.5194/acp-12-779-2012, 2012.

Zhu, J., Wang, T., Talbot, R., Mao, H., Hall, C. B., Yang, X., Fu, C., Zhuang, B., Li, S., Han, Y., and Huang, X.: Characteristics of atmospheric Total Gaseous Mercury (TGM) observed in urban Nanjing, China, Atmos. Chem. Phys., 12, 12103–12118, doi:10.5194/acp-12-12103-2012, 2012.

Zhuang, B. L., Jiang, F., Wang, T. J., Li, S., and Zhu, B.: Investigation on the direct radiative effect of fossil fuel black-carbon aerosol over China, Theor. Appl. Climatol., 104(3–4), 301–312, doi:10.1007/s00704-010-0341-4, 2011.

Zhuang, B. L., Li, S., Wang, T. J., Deng, J. J., Xie, M., Yin, C. Q., and Zhu, J. L.: Direct radiative forcing and climate effects of anthropogenic aerosols with different mixing states over China, Atmos. Environ., 79, 349–361, doi:10.1016/j.atmosenv.2013.07.004, 2013b.

Zhuang, B. L., Liu, Q., Wang, T. J., Yin, C. Q., Li, S., Xie, M., Jiang, F., and Mao, H. T.: Investigation on semi-direct and indirect climate effects of fossil fuel black carbon aerosol over China, Theor. Appl. Climatol., 114, 651–672, doi:10.1007/s00704-013-0862-8, 2013a.

Zhuang, B. L., Wang, T. J., Li, S., Liu, J., Talbot, R., Mao, H. T., Yang, X. Q., Fu, C. B., Yin, C. Q.,

752 Zhu, J. L., Che, H. Z., and Zhang, X. Y.: Optical properties and radiative forcing of urban aerosols
753 in Nanjing, China, Atmos. Environ., 83, 43–52, 2014a.
754 Zhuang, B. L., Wang, T. J., Liu, J., Li, S., Xie, M., Yang, X. Q., Fu, C. B., Sun, J. N., Yin, C. Q., Liao, J.
755 B., Zhu, J. L., and Zhang, Y.: Continuous measurement of black carbon aerosol in urban Nanjing of
756 Yangtze River Delta, China, Atmos. Environ., 89, 415–424, 2014b.
757 Zhuang, B. L., Wang, T. J., Liu, J., Ma, Y., Yin, C. Q., Li, S., Xie, M., Han, Y., Zhu, J. L., Yang, X. Q.,
758 and Fu, C. B.: Absorption coefficient of urban aerosol in Nanjing, west Yangtze River Delta, China,
759 Atmos. Chem. Phys., 15, 13633–13646, 2015.

760 **Figure captions:**

761 Figure 1. The 10th, 25th, median, 75th, and 90th percentiles of 550 nm AAC (a, Mm^{-1}), 470/660 nm
762 AAE (b), 550 nm SC (c, Mm^{-1}), 550 nm (d, Mm^{-1}) and 450/635 nm SAE (e) in each season from March
763 2014 to Feburay 2016.

764 Figure 2. Seasonal means (markers) and corresponding standard deviations (error bars) of wavelength
765 dependent AAC (a, Mm^{-1}), SC (b, solid mark, Mm^{-1}), Bsp (b, open mark, Mm^{-1}), EC (c, Mm^{-1}), SSA (e)
766 and ASP (f) at 450, 532, 550, 635 nm, as well as AAE at 470/660 nm (d, red solid mark) and SAE at
767 450/635 nm (d, green open mark)

768 Figure 3. Diurnal variations of 550 nm AAC (a, Mm^{-1}), SC (b, Mm^{-1}), Bsp (c, Mm^{-1}), SSA (d), ASP (g),
769 470/660 nm AAE (e) and 450/635 nm SAE (f) during the study period.

770 Figure 4. Frequency (%) distributions of 550 nm AAC (a), SC (b), Bsp (c), SSA (d), ASP (g), 470/660
771 nm AAE (e) and 450/635 nm SAE (f) on annual (shaded bar) and seasonal (markers in colors) scales.

772 Figure 5. Clusters of 96-h back trajectories arriving at the study site at 100 m in JJA (a) and DJF (b)
773 simulated by the HYSPIT model. The means with standard deviations of the aerosol optical properties

774 at each cluster of back trajectories in both JJA and DJF are plotted in Fig. 5c and 5d, respectively.

775 Figure 6. Relationships between 550 nm AAC and SC (solids square in blue) and between 550 nm Bsp

776 and SC (solid cycles in gray) in spring (a), summer (b), autumn (c) and winter (d).

777 Figure 7. Relationships between the 550 nm ASP and SC in different RH levels.

778 Figure 8. Relationships between the monthly mean values of 491 nm SSA and extinction Angstrom

779 exponent (EAE) at 491/863 nm (a) and between the monthly mean values of SSA difference (863-491

780 nm) and EAE at 491/863 nm (b).

781 Figure 9. Seasonal variations of RH (a, %) and linear correlations between AAE and RH (b, light blue,

782 upper), between SAE and RH (b, green, middle), and between ASP and RH (c, deep blue, lower).

783 Figure 10. Relationships between SC and visibility (open cycles) and between EC and visibility (solid

784 cycles) in different RH levels in spring (a), summer (b), autumn (c) and winter (d).

785 Figure 11. Relationships between SSA and visibility (solid cycles) and between ASP and visibility

786 (solid squares) in different RH and AAE levels in spring (a), summer (b), autumn (c) and winter (d).

787 Figure 12. Relationships between surface EC at 550 nm and column AOD at 500 nm in spring (a),

788 summer (b), autumn (c) and winter (d).

789

790 **Table captions:**

791 Table 1 Statistical summary of the surface aerosol optical properties in Nanjing.

792 Table 2 Seasonal mean±SD of the surface aerosol optical properties in Nanjing.

793 Table 3. The dominant and maximum frequencies as well as corresponding ranges of the aerosol

794 optical properties.

795 Table 4 The aerosol optical properties in Nanjing and at other sites of China.

796 Table 1 Statistical summary of the surface aerosol optical properties in Nanjing

Factors	Max	Min	Mean±SD	Median
550 nm AAC (Mm^{-1})	230.648	1.439	29.615±20.454	24.572
550 nm SC (Mm^{-1})	2493.092	20.673	338.275±228.078	284.379
550 nm Bsp (Mm^{-1})	300.101	1.401	44.257±27.396	38.206
550 nm EC (Mm^{-1})	2643.101	31.186	381.958±252.271	321.679
550 nm SSA	0.988	0.404	0.901±0.049	0.908
550 nm ASP	0.908	0.118	0.571±0.088	0.582
470/660 nm AAE	3.256	0.145	1.583±0.228	1.592
450/635 nm SAE	3.344	0.162	1.320±0.407	1.317

797 AAC: Aerosol absorption coefficient

798 SC: Aerosol scattering coefficient

799 Bsp: Aerosol back scattering coefficient

800 SSA: Aerosol single scattering albedo

801 ASP: Aerosol asymmetry parameter

802 AAE: Ångström exponent of absorbing aerosols

803 SAE: Ångström exponent of scattering aerosols

804

805 Table 2 Seasonal mean±SD of the surface aerosol optical properties in Nanjing

Factors	MAM	JJA	SON	DJF
550 nm AAC (Mm^{-1})	26.954±18.632	19.653±15.689	33.474±19.686	37.958±21.892
550 nm SC (Mm^{-1})	318.998±202.264	340.865±226.151	294.624±200.052	385.137±255.282
550 nm Bsp (Mm^{-1})	42.995±23.580	36.990±25.067	38.684±23.017	54.786±30.974
550 nm EC (Mm^{-1})	341.279±209.315	370.236±248.125	351.887±244.267	422.569±273.565
550 nm SSA	0.915±0.043	0.933±0.049	0.874±0.053	0.890±0.040
550 nm ASP	0.553±0.086	0.638±0.069	0.566±0.079	0.540±0.083

470/660 nm AAE	1.571±0.172	1.488±0.263	1.524±0.277	1.701±0.156
450/635 nm SAE	1.097±0.320	1.337±0.428	1.544±0.352	1.235±0.383

806

807 Table 3. The dominant and maximum frequencies as well as corresponding ranges of the aerosol
808 optical properties.

The aerosol optical properties	The dominant		The maximum	
	Bins	Frequencies	Bins	Frquencies
AAC	9~45 Mm^{-1}	73%	9~21 Mm^{-1}	32.9%
SC	60~390 Mm^{-1}	67%	170~280 Mm^{-1}	24.04%
Bsp	15~60 Mm^{-1}	69%	30~45 Mm^{-1}	26.45%
SSA	0.87~0.97	73%	0.91~0.93	18.64%
AAE	1.4~1.8	71%	1.5~1.6	20.9%
SAE	0.96~1.68	62%	1.32~1.5	18.06%
ASP	0.48~0.69	81%	0.55~0.62	34%

809

Table 4 The aerosol optical properties both in Nanjing and at other sites of China

Site	Period	AAC (Mm^{-1})	SC (Mm^{-1})	ASP	SSA	Method	References
Nanjing (urban)	2014.3-2016.2	29.6 (550 nm)	338.3 (550 nm)	0.57 (550 nm)	0.9 (550 nm)	[a] AE-31 [b] Aurora 3000	This stuty
Beijing (urban)	2005-2006	56 (532 nm)	288 (525 nm)	/	0.8 (525 nm)	[c] AE-16 [d] M9003	He et al. (2009)
Beijing (rural)	2003-2005	17.5 (525 nm)	174.6 (525 nm)	/	0.88 (525 nm)	[a] AE-31 [d] M9003	Yan et al. (2008)
Xi'an (urban)	2009	/	525 (520 nm)	/	/	[e] Auroral 1000	Cao et al. (2012)
Chengdu (urban)	2011	96 (532 nm)	456 (520 nm)		0.82	[a] AE-31 [f] Aurora 1000G	Tao et al. (2014)
Wuhan (urban)	2009.12-2014.03	119 (520 nm)	377 (550 nm)	/	0.73 (520 nm)	[a] AE-31 [g] Model 3563	Gong et al. (2015)
Xinken (rural)	2004.10-2011.05	70 (550 nm)	333 (550 nm)	/	0.83 (550 nm)	[h] MAAP [g] Model 3563	Cheng et al. (2008)
Tongyu (rural)	Spring, 2010 Spring, 2011	7.61 (520 nm) 7.01 (520 nm)	89.2 (520 nm) 85.3 (520 nm)	/ /	0.9 (520 nm)	[a] AE-31 [b] Aurora 3000	Wu et al. (2012)
Nanjing (suburban)	2011.03-04	28.1 (532 nm)	329.3 (550 nm)	/	0.89 (532 nm)	[i] PASS [d] Model 3563	Yu et al. (2016)
Shanghai (ruban)	2010.12-2011.03	66 (532 nm)	293 (532 nm)	/	0.81 (532 nm)	[a] AE-31 [g] Model 3563	Xu et al. (2012)
Shouxian (rural)	2008.5-12	29 (550 nm)	401 (550 nm)	/	0.92 (550 nm)	[j] Model PSAP [g] Model 3563	Fan et al. (2010)
Lanzhou (urban)	Winter 2001, 2002	/	226 (550 nm)	/	/	[d] Model 3563	Zhang et al. (2004)
Panyu (urban)	Spring and winter, 2008	84.03 and 188.8 (532 nm)	/	/	/	[a] AE-31	Wu et al. (2013)
Dongguan (suburban)	Spring and winter, 2008	47.1 and 95.53 (532 nm)	/	/	/	[a] AE-31	Wu et al. (2013)

Maofengshan (Rural)	Spring and winter, 2008	26.45 and 28.77 (532 nm)	/	/	/	[a] AE-31	Wu et al. (2013)
Yongxing Island	Spring and winter, 2008	7.21 and 8.37 (532 nm)	/	/	/	[a]AE-31	Wu et al. (2013)

[a] Seven channels Aethalomter (model AE-31, Magee Scientific, USA)

[b] Three wavelength integrating Nephelometer (Model Aurora 3000, Australia)

[c] Aethalometer AE16

[d] Nephelometer M9003

[e] Integrating Nephelometer (Model Aurora 1000)

[f] Integrating Nephelometer (Model Aurora 1000G)

[g] Integrating Nephelometer (Model 3563, TSI, USA)

[h] Multi-angle Absorption Photometer (MAAP, Thermo, Inc., Waltham, MA USA, Model 5012)

[i] Photo acoustic Soot Spectrometer (PASS 1, DMT, USA)

[j] Particle/SootAbsorption Photometer

Figures:

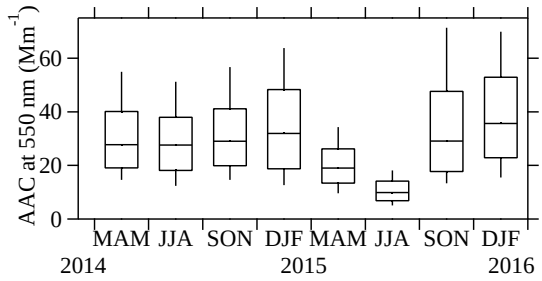

a)

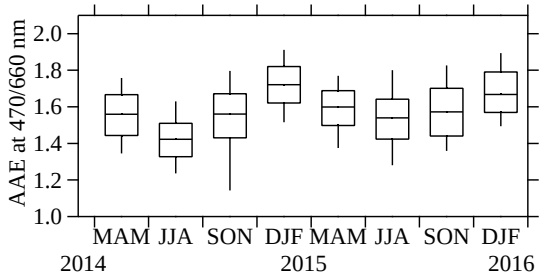

b)

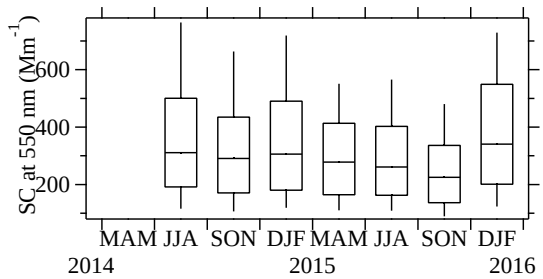

c)

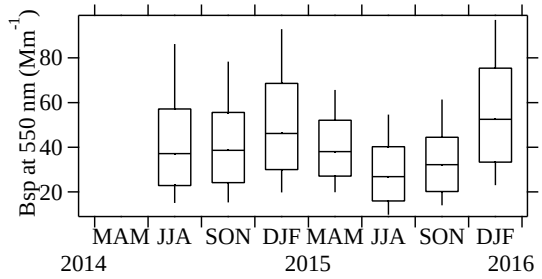

d)

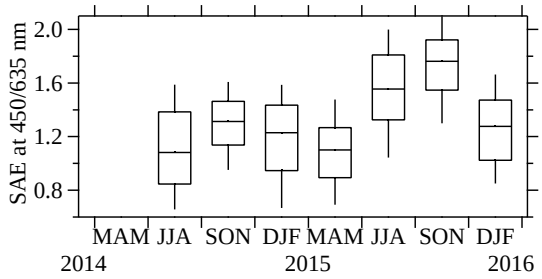

e)

Figure 1.

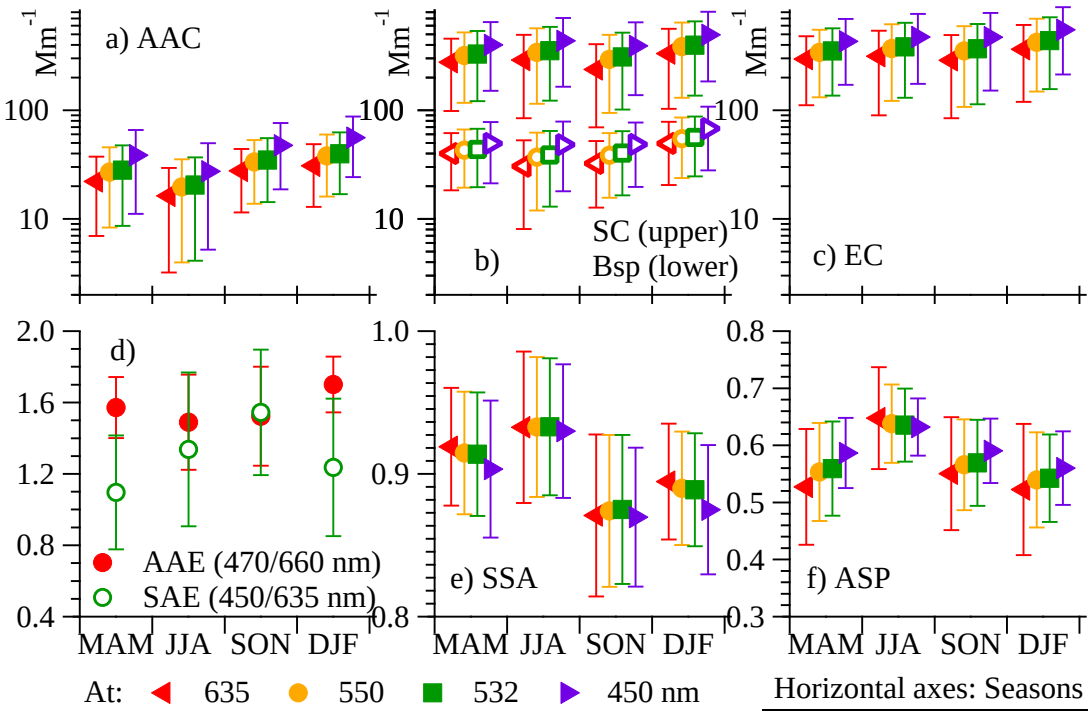

Figure 2.

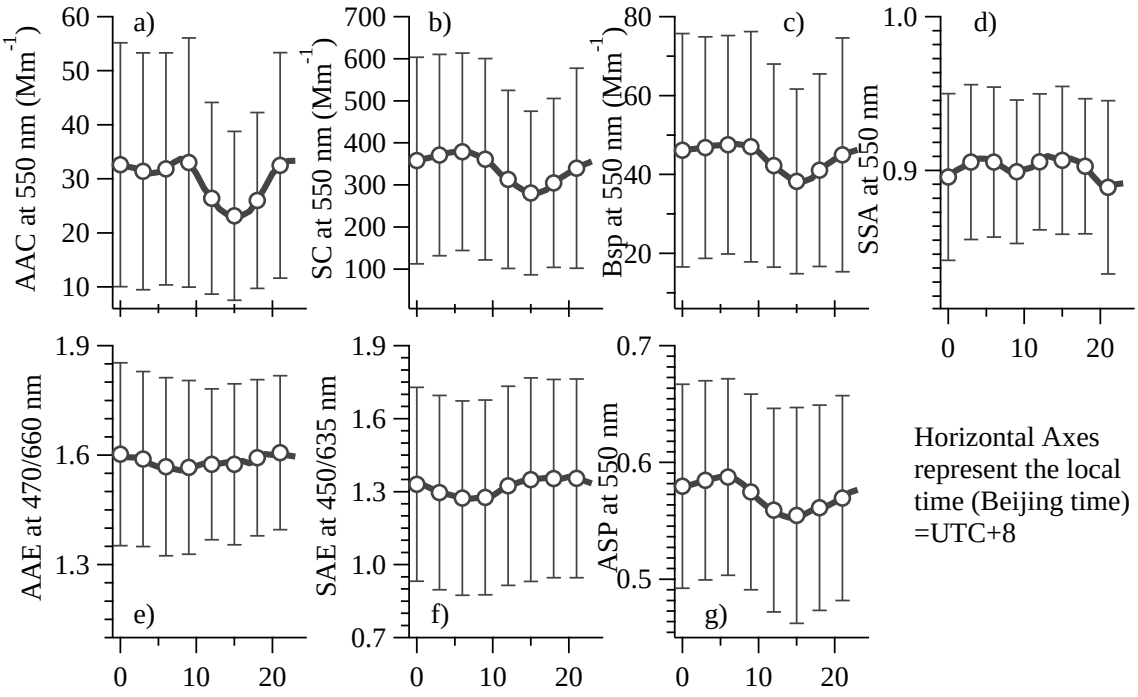

Figure 3

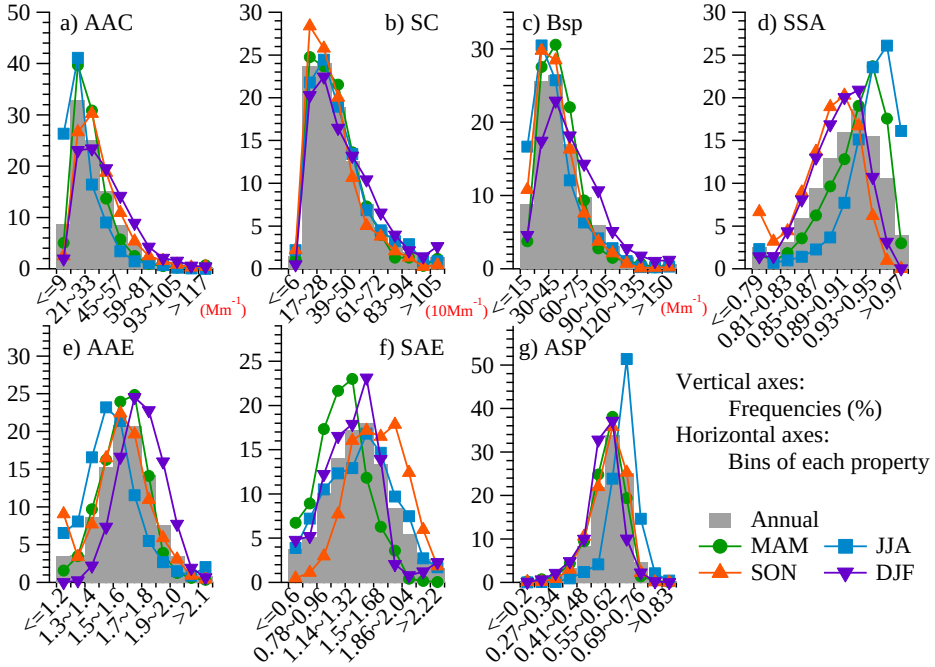

Figure 4

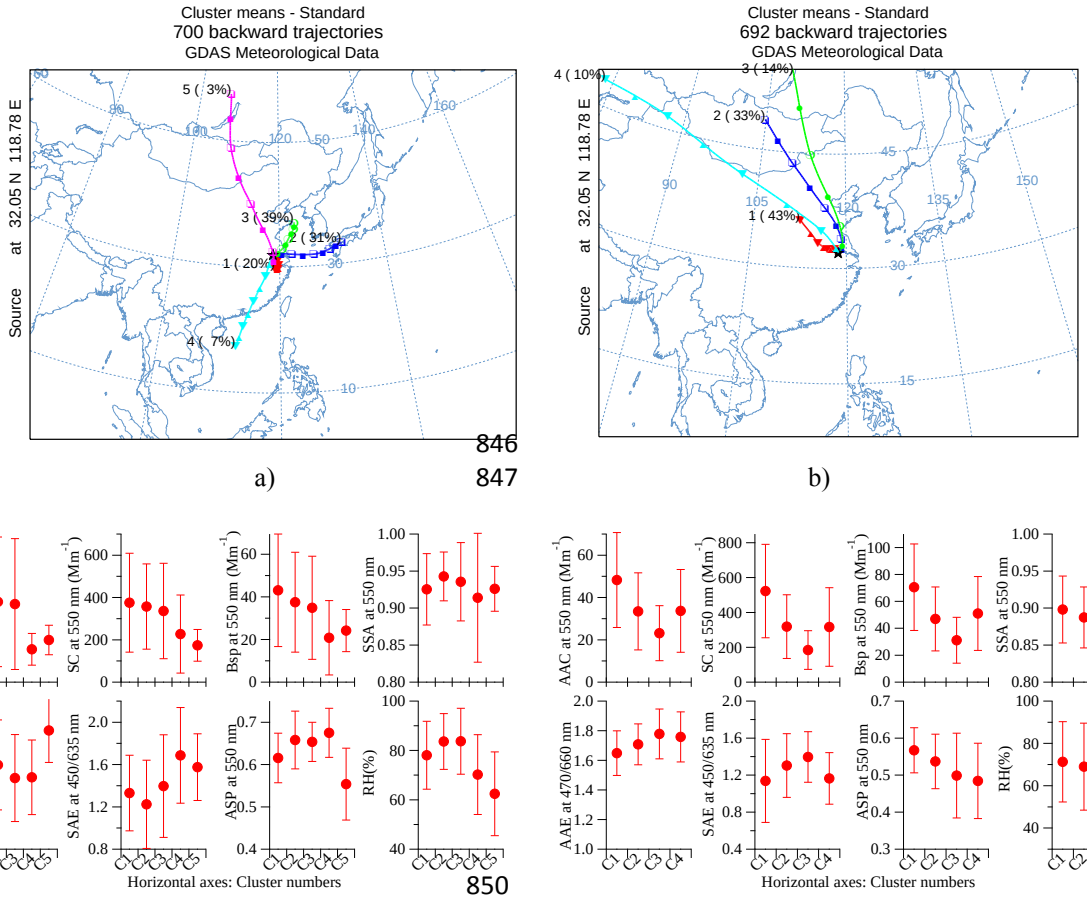

Figure 5

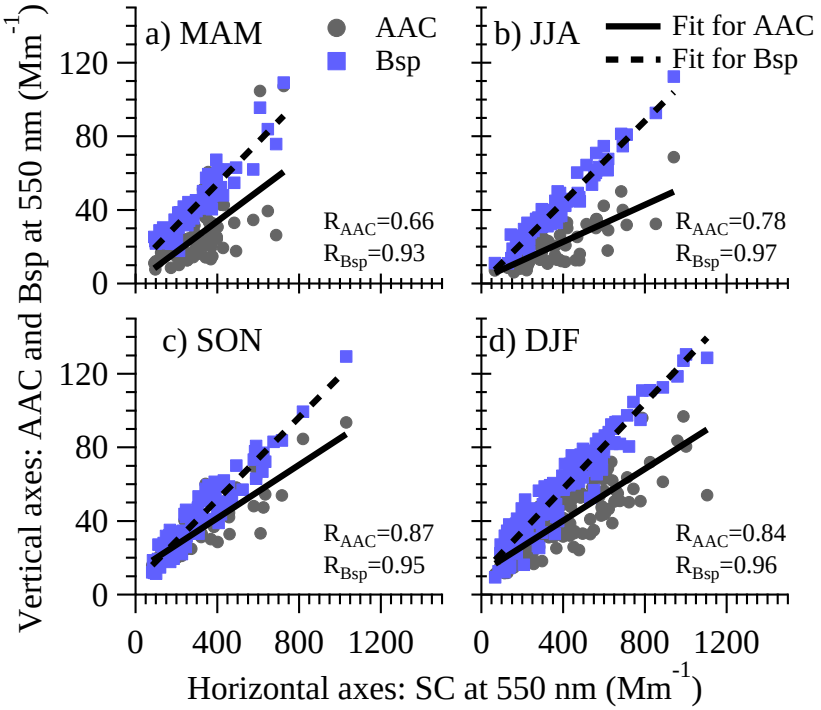

Figure 6

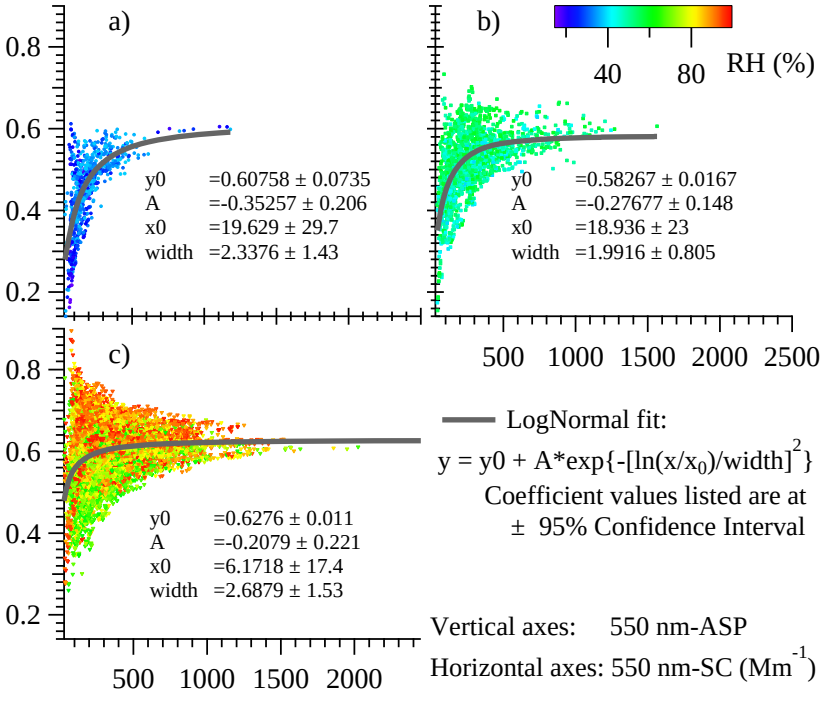

Figure 7

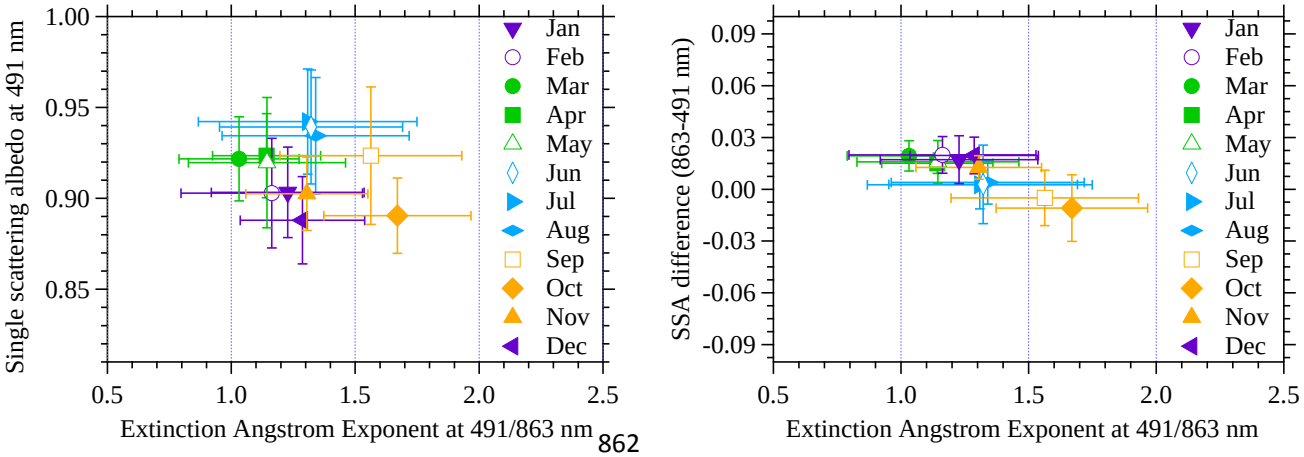

a) b)

Figure 8

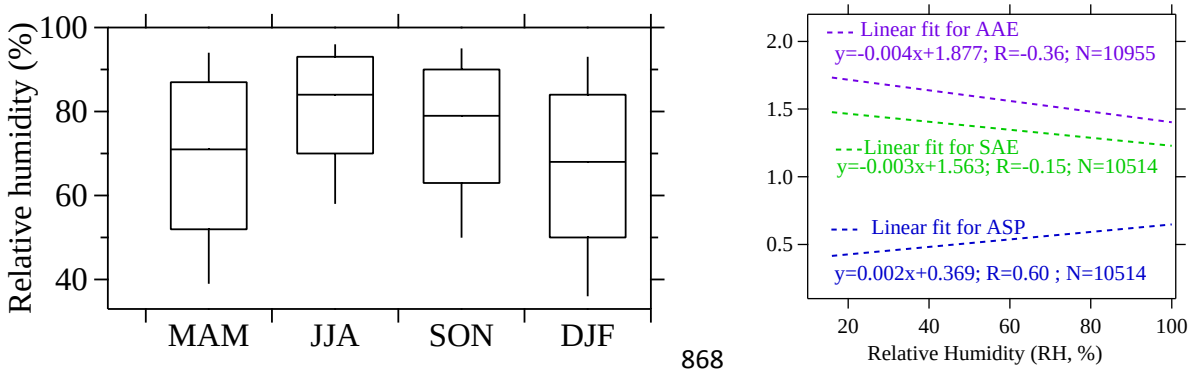

a) b)

Figure 9

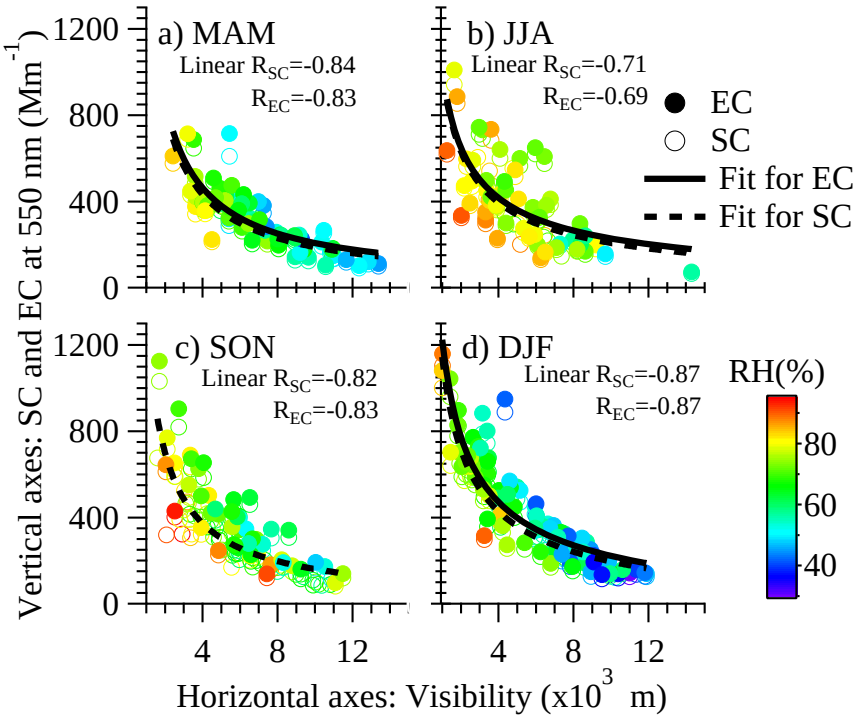

871

872 Figure 10

873

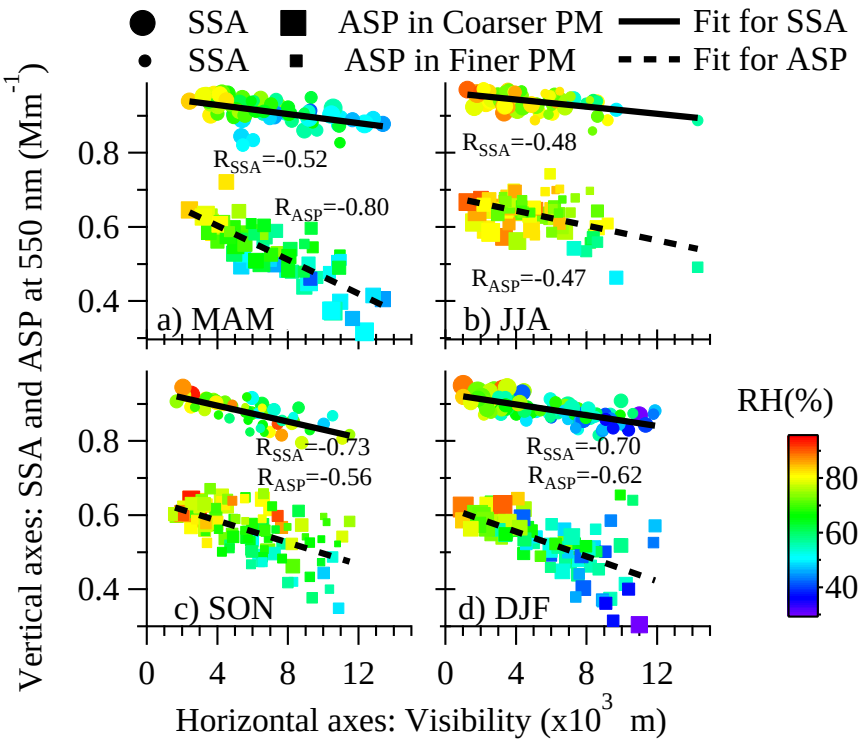

874

875 Figure 11

876

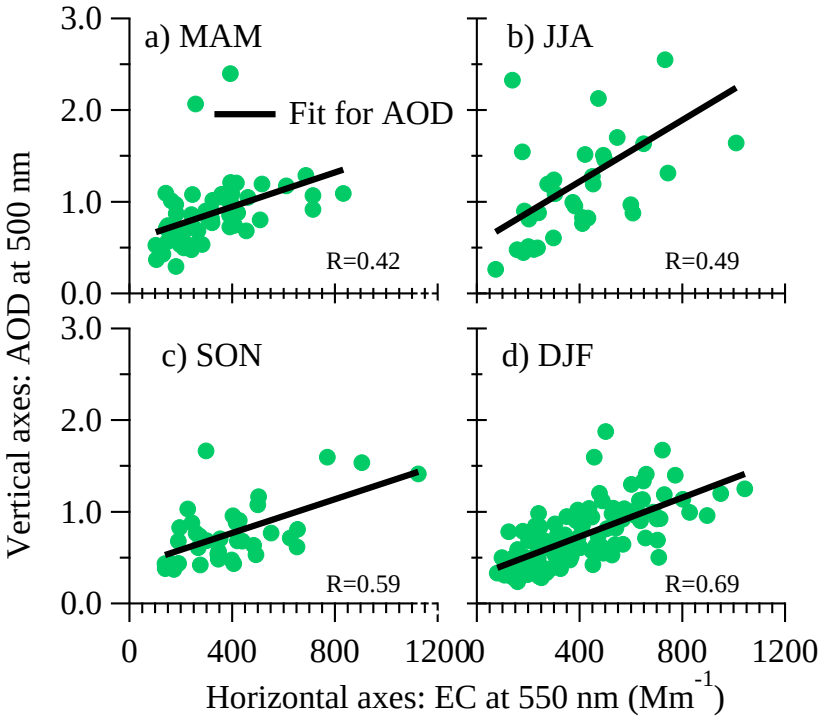

877

878 Figure 12